Chapter 3

Isolation, Semi-synthetic Modification, and Cytotoxic Evaluation of Compounds of *Gloriosa superba* Roots

3. Isolation, semi-synthetic modification, and cytotoxic evaluation of compounds of *Gloriosa superba* roots

3.1. Literature review

Gloriosa superba (Family: Colchicaceae), commonly known as 'glory lily', is an herbaceous climber plant native to tropical Asia and Africa. The plant is distributed throughout tropical India, from the Himalayan ranges to Assam and Deccan peninsula, extending up to an altitude of 2000 m. This plant is industrially employed for the commercial production of colchicine, due to which it was under the threatened category. However, it is presently cultivated in Tamil Nadu and other parts of south India to fulfill industrial demands (Singh, 2006). This valuable plant is also propagated by a number of botanical research institutes and nurseries. Due to the fascinating flower of Glory lily, it is also used as an ornamental plant in gardens. The roots of *G. superba* are used traditionally in the Indian System of Medicine for the treatment of gout, arthritis, rheumatic disorders, skin diseases, leprosy, ulcers, snakebite, impotency, etc. (Jana and Shekhawat, 2011). In the Ayurveda, *G. superba* has been mentioned as one of the seven upavishas i.e. semi-poisonous drugs. The poisoning by tubers of *G. superba* caused marked alopecia, diarrhea, and menorrhagia due to its high colchicine content (Gooneratne, 1966). The *G. superba* extract has shown antimicrobial (Khan et al., 2008), analgesic, anti-inflammatory (John et al., 2009), antioxidant (Bahukhandi et al., 2021), and anticancer (Olowofolahan and Olorunsogo, 2021) activities. The alcoholic extract of its roots and its fractions showed enzyme inhibition activities against lipoxygenase, acetylcholinesterase, and butyrylcholinesterase (Khan et al., 2007). The ethanolic extract of *G. superba* leaves has shown the anticancer potential by inducing mitochondrial permeability transition (mPT) pore opening, and protect against monosodium glutamate-induced proliferative disorder (Olowofolahan and Olorunsogo,

2021). Some nano-formulations using *G. superba* root extract have also exhibited anticancer activity against MCF-7 (human breast adenocarcinoma) cell line (Rokade et al., 2018; Ghosh et al., 2016). Thirty one compounds have been reported to be isolated from *G. superba* such as 6-methoxysalicylic acid (**3.1**), colchicine (**3.2**), gloriosine (**3.3**), 3-demethyl colchicine (**3.4**), 3-demethyl gloriosine (**3.5**), β-lumicolchicine (**3.10**), colchicoside (**3.12**) etc. (Figure 3.1).

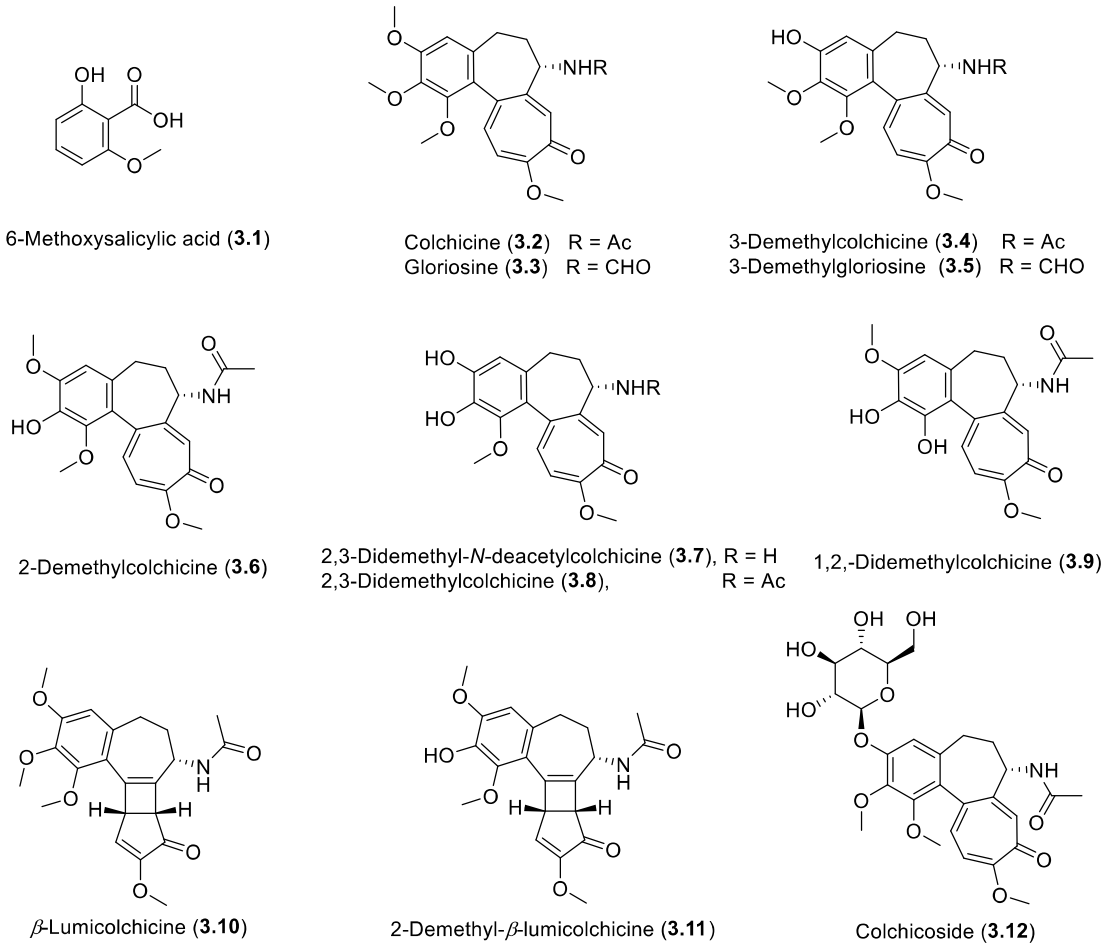

Figure 3.1. Reported compounds from *Gloriosa superba* roots

Colchicine (**3.2**) is a privileged natural product, reported from the *Colchicum autumnale* and *Gloriosa superba*, which has been long used for the treatment of gout, familial Mediterranean fever, and Behçet's disease. A semisynthetic derivative of colchicine,

thiocolchicoside, is a muscle relaxant used clinically as an anti-inflammatory and analgesic drug (Carta et al., 2006). Colchicine exhibits potential anti-proliferative activity by binding to colchicine binding site (CBS) of tubulin protein (Figure 3.2) and inhibiting its self-assembly and microtubule polymerization and thereby arresting cell division (Kumar et al., 2017). It has also advanced into various stages of clinical trials for the treatment of different type of cancer, and various cardiovascular disorders (Verma et al., 2015; Deftereos et al., 2013). Colchicine develops multi-drug resistance due to its p-glycoprotein induction activity (Singh et al., 2015). Also, it has shown potential toxic effects like cardiotoxicity, neuropathy, myopathy due to its toxicity (Kuncl et al., 1987; Tochinai et al., 2014). These factors limited the clinical use of colchicine as an anticancer drug.

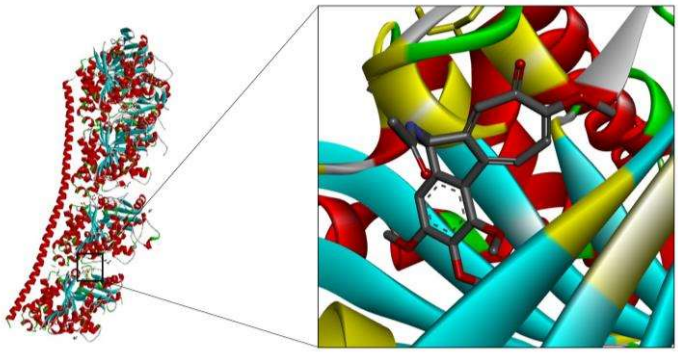

Figure 3.2. Colchicine at the colchicine-binding site located between α- and β-subunits of the tubulin protein

3.1.1. SAR of colchinoids

Structurally, colchicine (**3.2**) consists of a trimethoxyphenyl ring (A), a cycloheptane ring (B), and a tropolone ring (C). As shown in the Figure 3.2, colchicine bind to the colchicine binding site located at the interphase between α- and β-subunits of tubulin heterodimer. Rings A and C are essential pharmacophores for tubulin binding. The three methoxy groups at C-1, C-2, and C-3 of ring A play a crucial role in the high affinity of

colchicine towards tubulin protein. Podophyllotoxin acts a competitive inhibitor of colchicine due to the presence of trimethoxyphenyl ring. Substitution of any of the methyl groups with bulky groups (as in colchicoside) results in reduced affinity for tubulin. At the same time when any one or more methoxy groups are demethylated, antimitotic activity is greatly affected. Various C-4 substituted derivatives were synthesized and it was found that 4-halo derivatives showed potential activity towards tumor cells A549, HT29, and HCT116 (Yasobu et al., 2011). In another study, C-4 halo substituted thiocolchicine derivatives showed nonomolar potency in all the investigated cell lines (A549, MCF-7, LoVo) and a higher selectivity towards cancer cells over normal cells (Majcher et al., 2018b).

Although ring B is not essential for tubulin binding, it plays an important role in the kinetic properties of the colchicine-tubulin binding. Nitrogen at C-7 is essential for the recognition by P-gp. Substitution at C-7 is well tolerated by tubulin. Acetamide group at C-7 can be replaced by other substituents like amides, urea, thiourea, carbamates, 1,2,3-triazoles, etc. maintaining the cytotoxic activity (Kim et al., 2013; Krzywik et al., 2021; Zhang et al., 2015; Majcher et al., 2018a).

The tropolone ring (ring C) of colchicine is an important structural feature for its cytotoxic activity. The relative positions of C-9 ketone and C-10 methoxy group are important for the tubulin binding. Isocolchicine with reversed carbonyl and methoxy groups' relative position is inactive. Photo-isomer of colchicine called as lumicolchicine possess a transformed ring C (4- and 5-membered rings fused system) and have reduced binding affinity towards tubulin. Substitution of different amines at C-10 position resulted in potent compounds with significantly reduced P-gp induction liability (Singh et al., 2015). Ring C can be modified with different N,O-containing heterocyclic and/or aliphatic substitutions to

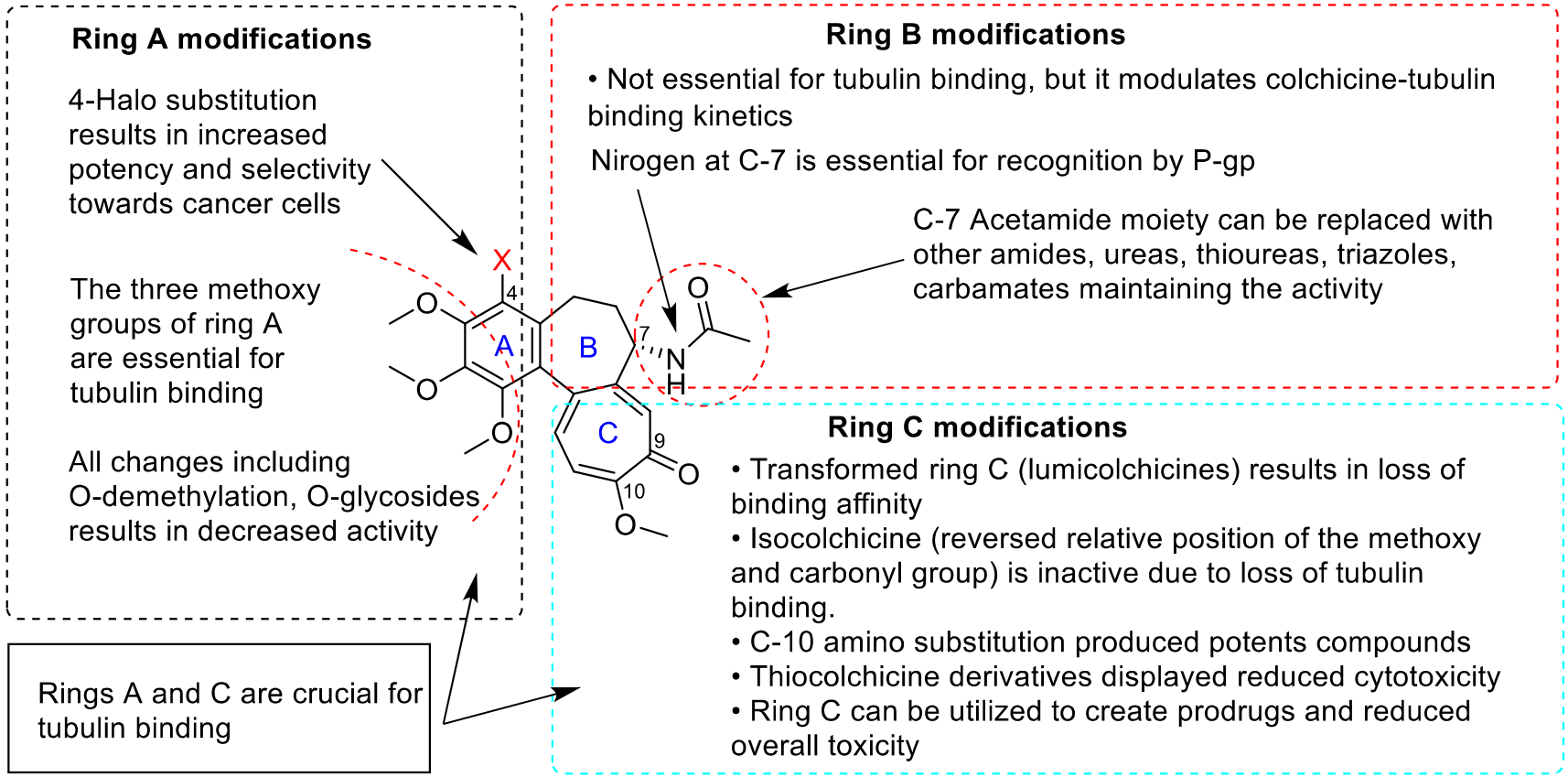

Figure 3.3. Structure-Activity Relationship (SAR) studies of colchinoids

create prodrugs and reduced overall toxicity (Figure 3.3).

Despite having remarkable anticancer potential, colchicine couldn't pave its way to the clinic. At the same time, gloriosine is yet to be investigated for its pharmacology. In our continuous search for anticancer leads, the roots of *G. superba* were investigated for phyto-chemistry and medicinal chemistry. We carried out preliminary cytotoxic screening of gloriosine in 15 human cancer cell lines and one normal cell line. Further, new semi-synthetic derivatives of gloriosine were synthesized.

3.2. Results and discussion

3.2.1. Phytochemistry of *Gloriosa superba* roots

The dried roots of *G. superba* were extracted three times with chloroform:methanol (v/v, 1:1) at room temperature. The crude extract was concentrated under reduced pressure to evaporate the organic solvent. The dried extract was subjected to silica gel column chromatography. Repeated column chromatography led to the isolation of sixteen known and one new compound. All the known compounds were characterized by matching with their reported ^{1}H and ^{13}C NMR values. Isolated compounds were identified as stigmasterol (**2.15**), β-sitosterol (**2.16**) (Goel et al., 2021), trioxsalen (**3.13**), caffeic acid (**3.14**), 6-methoxysalicylic acid (**3.1**), *β*-lumicolchicine (**3.10**) (Meksuriyen et al., 1988), 2-demethyl-*β*-lumicolchicine (**3.11**), *N*-deacetyl-*N*-formyl-*β*-lumicolchicine (**3.15**), 3-demethyl-*β*-lumicolchicine (**3.16**), 3-demethyl-*N*-Deacetyl-*N*-formyl-*β*-lumicolchicine (**3.17**), γ-lumicolchicine (**3.18**) (Meksuriyen et al., 1988), colchicine (**3.2**) (Alali et al., 2005), gloriosine (**3.3**), 3-demethylcolchicine (**3.4**) (Alali et al., 2005), 3-demethylgloriosine (**3.5**), and colchicoside (**3.12**) (Zarev et al., 2017). The new compound **3.19** was characterized by extensive 2D NMR studies (Figure 3.4).

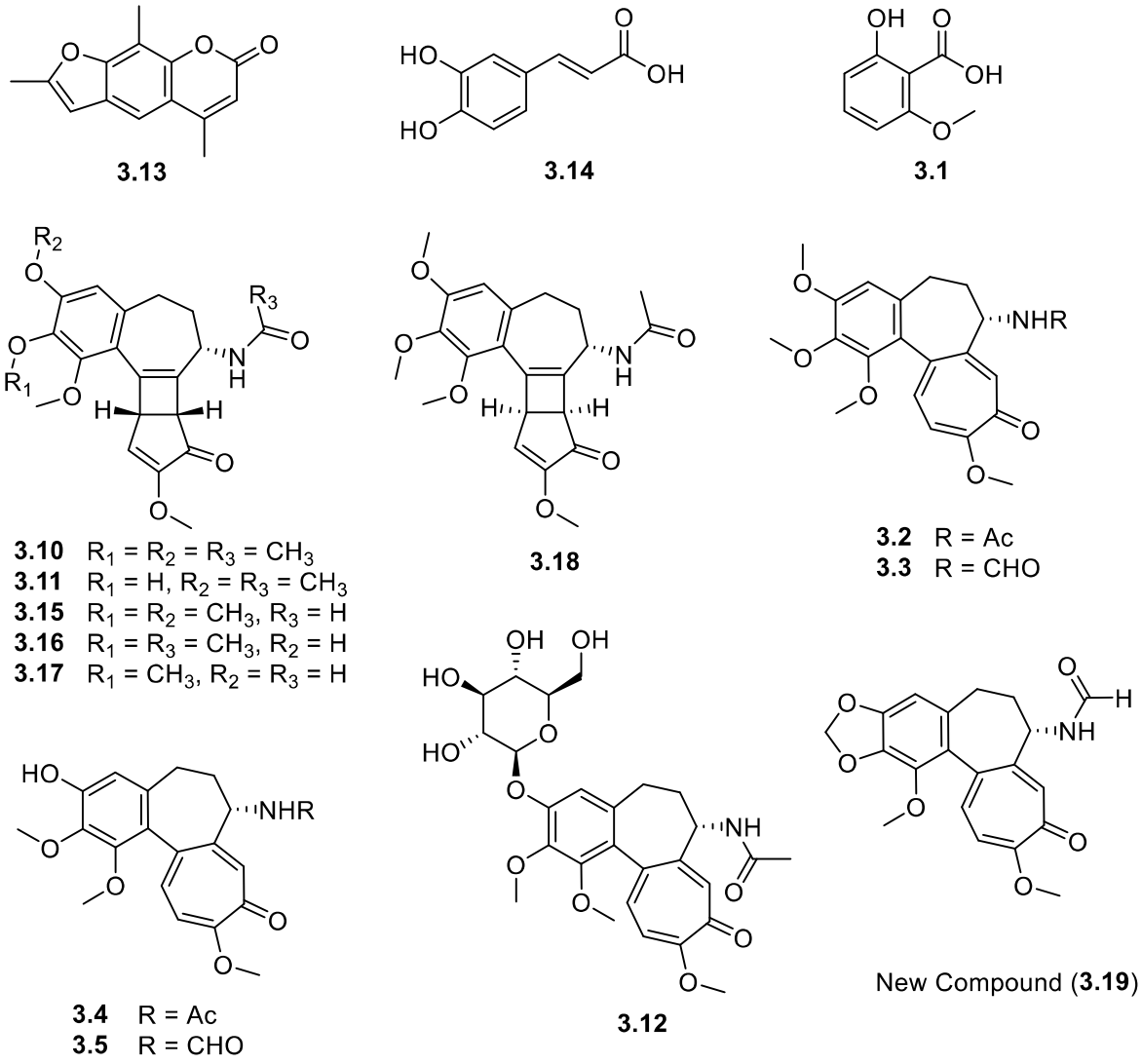

Figure 3.4. Isolated compounds from *G. superba* roots

Stigmasterol (**2.15**), *β*-sitosterol (**2.16**), trioxsalen (**3.13**), caffeic acid (**3.14**), and 6-methoxysalicylic acid (**3.1**) were non-alkaloidal common components widely reported from various higher plant species. *β*-Lumicolchicine (**3.10**), 2-demethyl-*β*-lumicolchicine (**3.11**), *N*-deacetyl-*N*-formyl-*β*-lumicolchicine (**3.15**), 3-demethyl-*β*-lumicolchicine (**3.16**), 3-demethyl-*N*-Deacetyl-*N*-formyl-*β*-lumicolchicine (**3.17**), and γ-lumicolchicine (**3.18**) were obtained as minor compounds. *β*- and *γ*-Lumicolchicine are stereoisomers with acetamide

group at C-7 in *cis*- or *trans*-configuration to the five-membered ring (with ring A, ring B, and four membered rings co-planar) (Forbes, 1955). Final structures of **3.10** and **3.18** were established by the NOESY experiments. In *β*-lumicolchicine (**3.10**), H-7 (δ_H 4.82 ppm) and H-8 (δ_H 3.62 ppm) displayed spatial correlation in NOESY spectra, but this correlation was not observed in γ-lumicolchicine (**3.18**), confirming that in **3.10** both H-7 and H-8 are *cis* to each other, whereas in **3.18** these protons are *trans* (Figure 3.5).

Lumicolchicines are the isomers of colchicine in which ring C of colchicine is rearranged to a conjugated 4- and 5-membered ring system. Although lumicolchicines have been isolated from *G. superba* earlier, they may be artifacts because lumicolchicines have been reported to be produced as a result of photoisomerization of colchicine when exposed to UV light. 3-Demethylcolchicine (**3.4**) (Alali et al., 2005), 3-demethylgloriosine (**3.5**), and colchicoside (**3.12**) were obtained in minor amounts from the polar fractions of column.

Repeated attempts were made to purify the gloriosine (**3.3**) as it is closely associated with colchicine (**3.2**). Isolate was characterized by NMR studies, ^{1}H NMR and ^{13}C NMR spectra of **3.2** and **3.3** were very similar. When NMR spectra of colchicine and gloriosine were compared, it was found that in gloriosine (**3.3**), methyl peaks δ_H 1.97 and δ_C 22.8 ppm were not observed (as in colchicine), while an aldehyde proton was detected at δ_H 8.18 ppm in gloriosine (Figure 3.6). Also, peak due to aldehyde carbonyl group appeared at δ_C 160.9 ppm in place of δ_C 170.1 ppm (peak due to acetamide carbonyl group in colchicine) (Figure 3.7). DEPT-135 and HSQC NMR spectra of gloriosine confirmed the presence of aldehyde group at δ_C 160.9 ppm (Figure 3.8). The complete structure of gloriosine (**3.3**) was established by 2D NMR. Based on these findings and validated by HRMS spectra, it is confirmed that chemically gloriosine (**3.3**) is *N*-deacetyl-*N*-formylcolchicine.

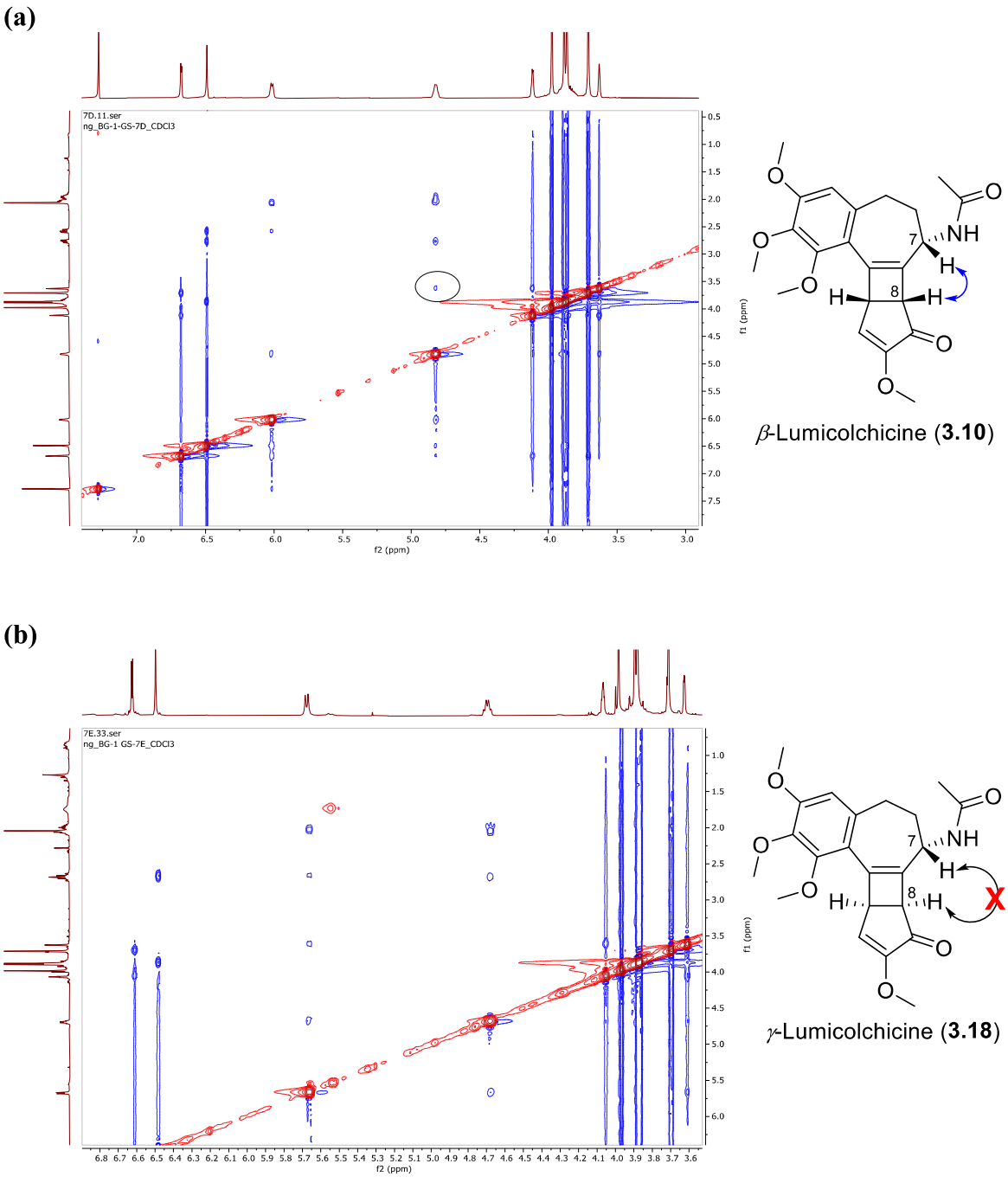

Figure 3.5. NOESY NMR spectra of *β*-lumicolchicine (**3.10**) and *γ*-lumicolchicine (**3.18**)

a

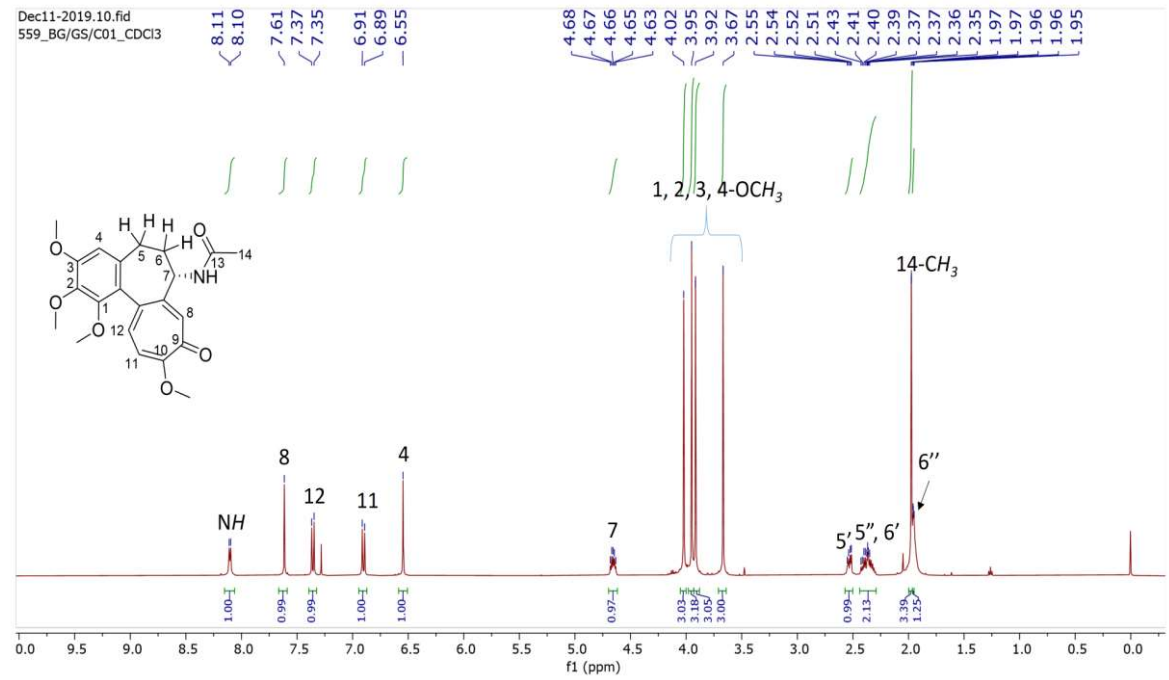

b

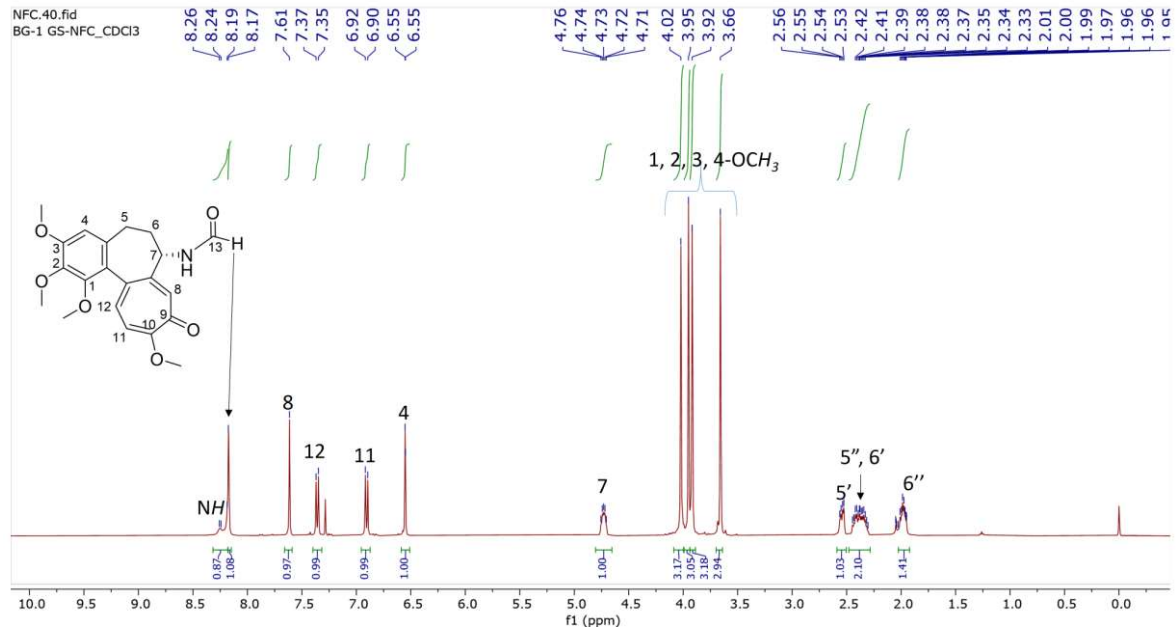

Figure 3.6. ^{1}H NMR spectra of (a) colchicine (**3.2**), and (b) gloriosine (**3.3**) in $CDCl_3$ (500 MHz). In gloriosine, methyl peak at 1.97 ppm is not observed, and a singlet at 8.17 ppm is observed due to aldehyde proton

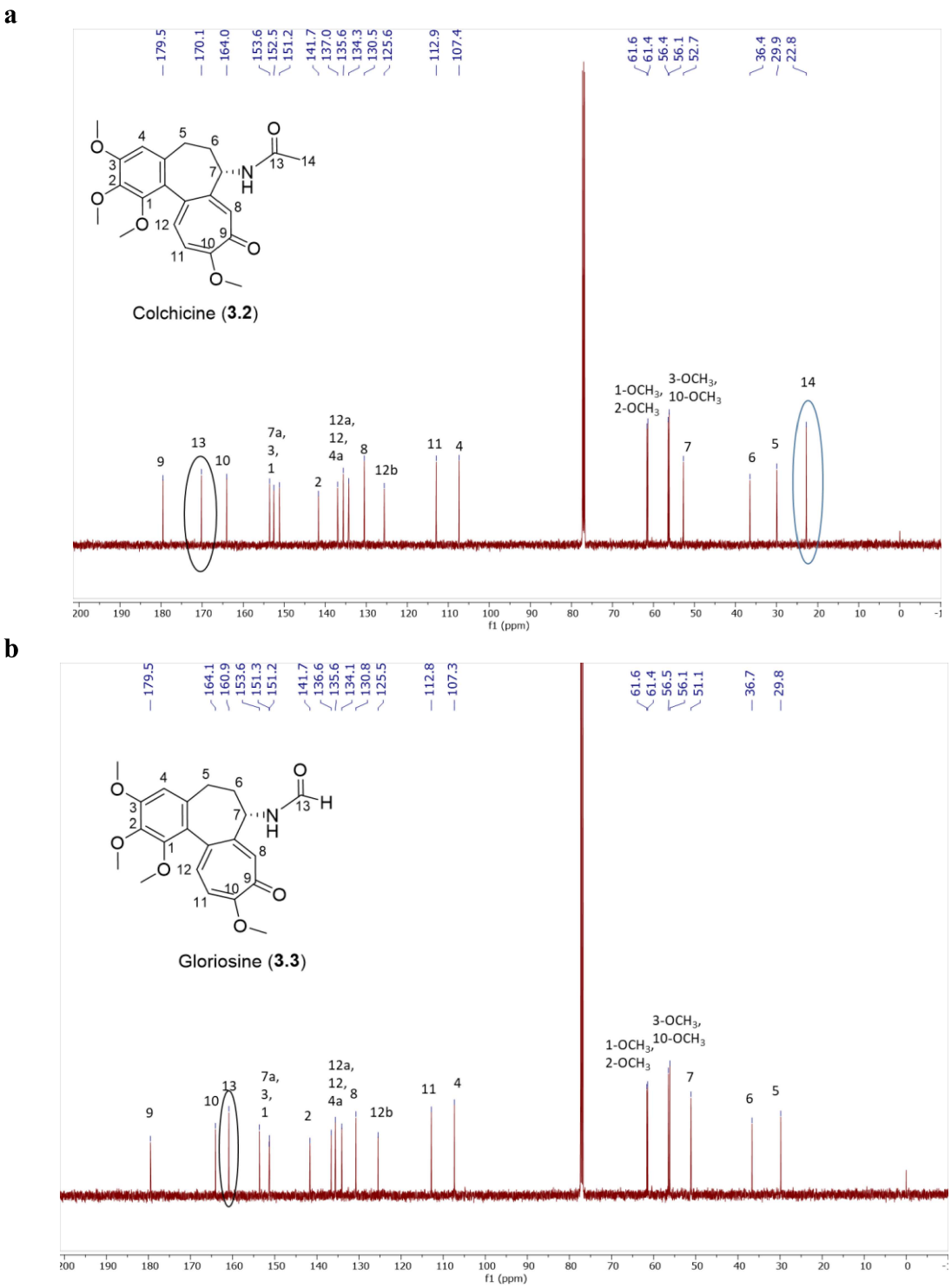

Figure 3.7. ^{13}C NMR spectra of (a) colchicine (**3.2**), and (b) gloriosine (**3.3**) in $CDCl_3$ (125 MHz). Peak due to aldehyde carbonyl group appeared at δ_C 160.9 ppm in gloriosine in place of δ_C 170.1 ppm (peak due to acetamide carbonyl group in colchicine).

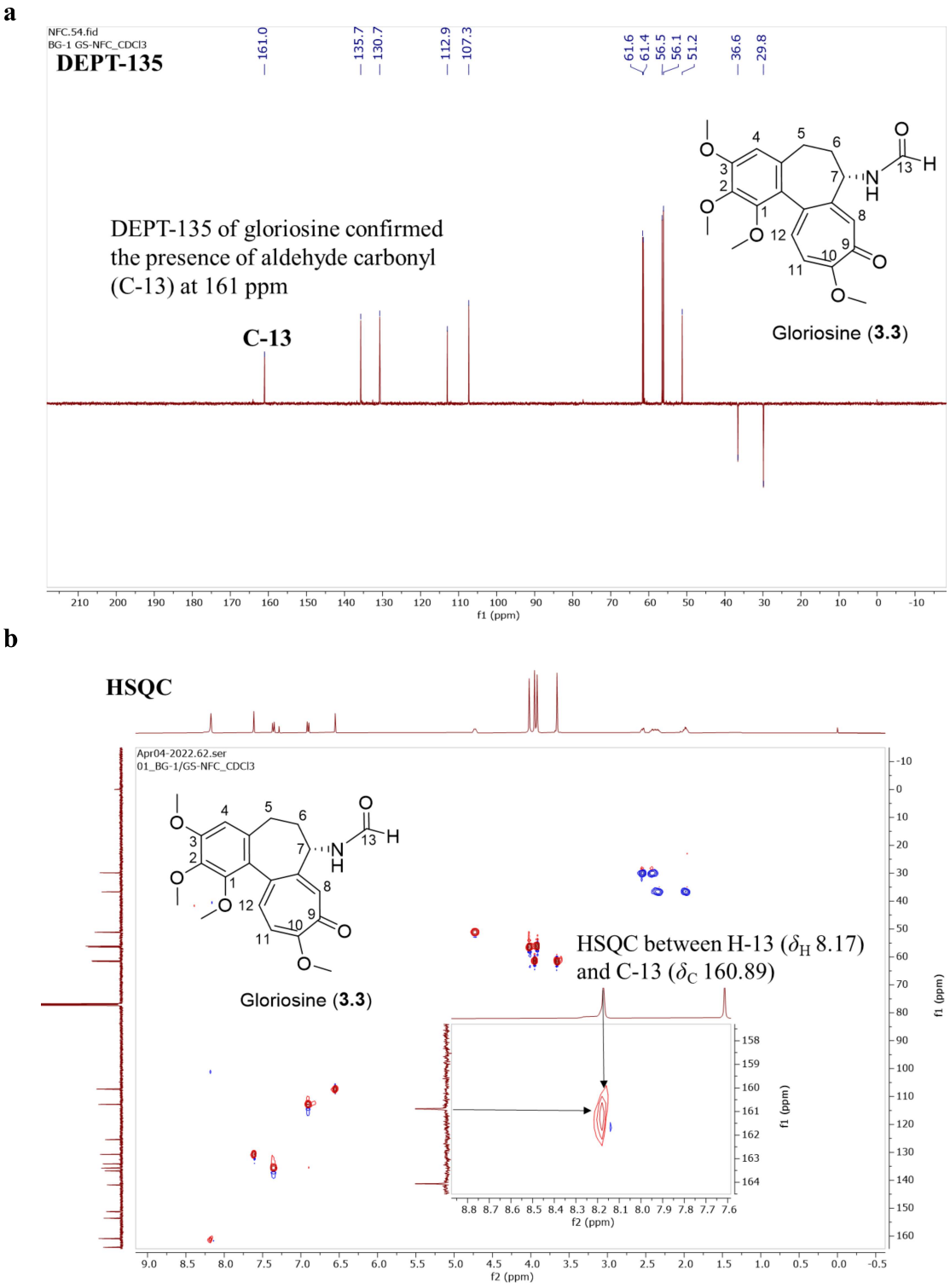

Figure 3.8. DEPT-135 and HSQC NMR spectra of gloriosine (**3.3**)

3.2.2. Structure elucidation of new compound (3.19)

Compound **3.19** (5 mg) was obtained as a buff coloured powder. The structure was established by extensive 2D NMR and HRMS experiments. The molecular formula of compound **3.19** was identified as $C_{20}H_{19}NO_6$ based on the HRMS (observed *m/z* $[M + H]^+$ 370.1282, calcd for $C_{20}H_{20}NO_6^+$, 370.1285). The complete ^1H, ^{13}C, DEPT-135, and HMBC data sets are shown in Table 3.1. The 1D NMR showed structural similarities with colchinoids, especially gloriosine (**3.3**). In particular, compound **3.19** differed from gloriosine (**3.3**) by the absence of two methoxyl groups. The characteristic peaks for a tropolone ring C, a ketone carbonyl at 179.41 ppm, two adjacent CH doublets at 6.84 and 7.25 ppm (AB pattern, H-11 and H-12 respectively), and a CH singlet at 7.46 ppm (C-8), were present and confirmed by NMR experiments (Figure 3.10). The methoxy singlet at 4.01 ppm showed HMBC correlation with C-10. Another methoxy group at 3.81/60.56 ppm showed HMBC correlation with C-1. One singlet at 6.01 ppm due to two hydrogen atoms showed HSQC correlation with a methylene carbon at 101.48 ppm, and HMBC correlations with C-2 and C-3 (Figure 3.11). Literature search showed that this pattern was like that of ring A of cornigerine (Alali et al., 2005). Thereby, the structure of **3.19** was established as *N*-deacetyl-*N*-formylcornigeririne, a new colchinoid analogue, and was named as glorigerine (Figure 3.9). On the basis of the well-known biosynthetic pathway for colchinoids, the stereochemistry at C-7 was assumed to be *S* (Maier and Zenk, 1997; Alali et al., 2005).

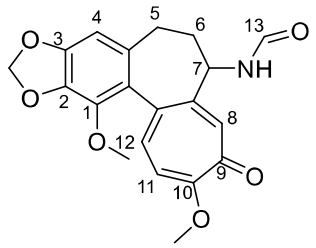

Figure 3.9. Chemical structure of new compound, glorigerine (**3.19**)

Table 3.1. NMR spectroscopic data for compound **3.19** in $CDCl_3$.

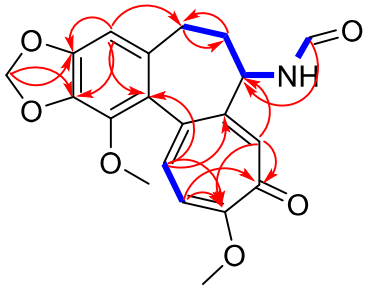

HMBC

^1H-^1H COSY

Position	δ_H	**mult (*J* in Hz)**	δ_C	**DEPT**	**HMBC**
1			140.9	C	
2			137.2	C	
3			149.2	C	
4	6.46	s	103.4	CH	C-5, 12b, 3, 2
4a			132.8	C	
5	2.32	m	29.7	CH_2	C-6, 4, 12b, 4a,
	2.49	m			
6	2.28	m	37.3	CH_2	C-5, 7, 7a
	1.82	m			
7	4.74	m	50.6	CH	
7a			150.6	C	
8	7.46	s	130.8	CH	C-7, 9, 10, 7a, 12a
9			179.4	C	
10			164.1	C	
11	6.84	d (10.9)	112.4	CH	C-12a, 10, 9
12	7.25	d (10.7)	135.6	CH	C-12b, 10, 7a
12a			136.0	C	
12b			125.1	C	
13	8.17	s	160.5	CH	C-7
1-OCH_3	3.81	s	60.6	CH_3	C-1
O-CH_2-O	6.01	s	101.5	CH_2	C-2, 3
10-OCH_3	4.01	s	56.4	CH_3	C-10
NH	6.94	d (7.5)			

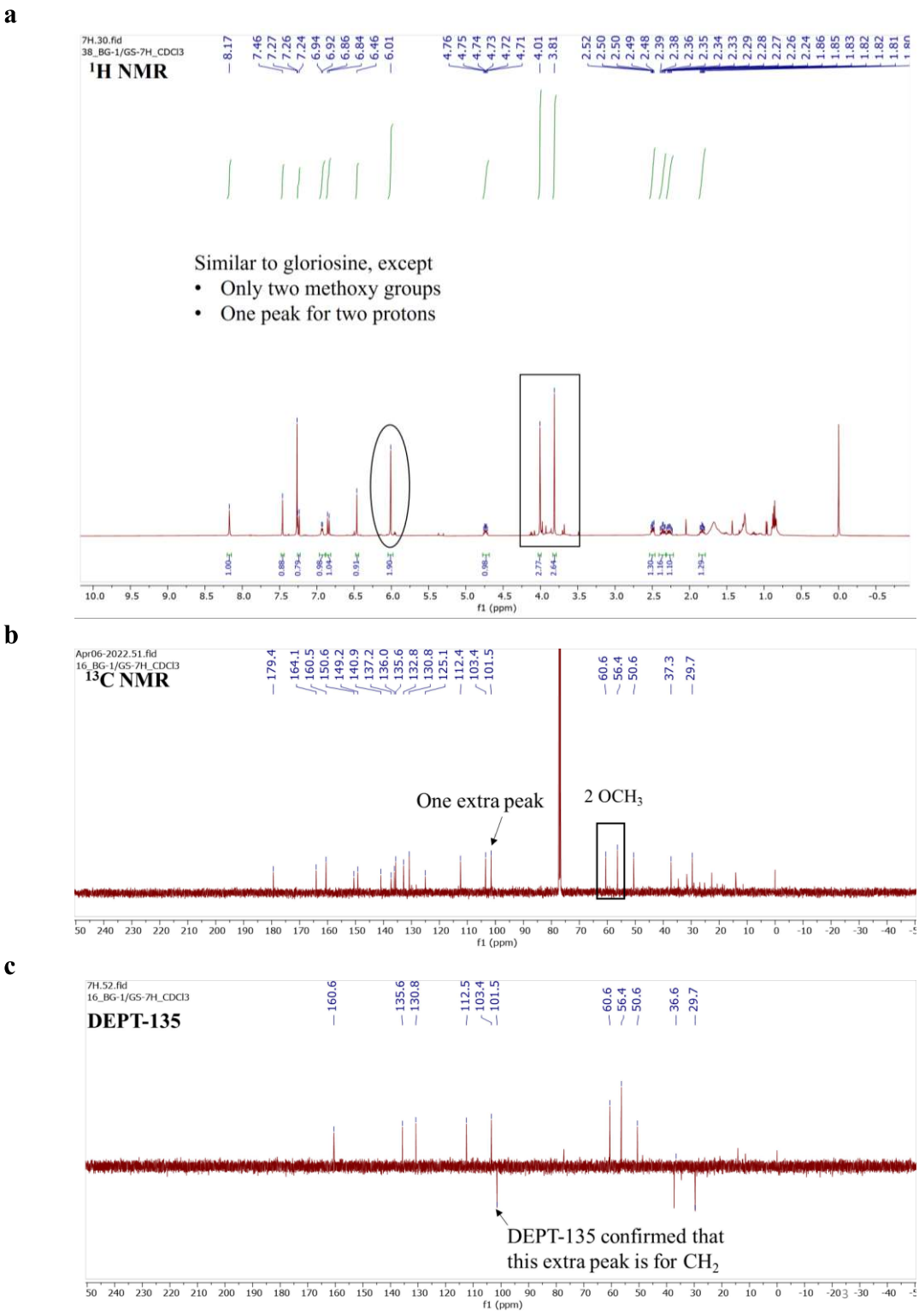

Figure 3.10. ^{1}H, ^{13}C, and DEPT-135 NMR spectra of new compound **3.19** in $CDCl_3$

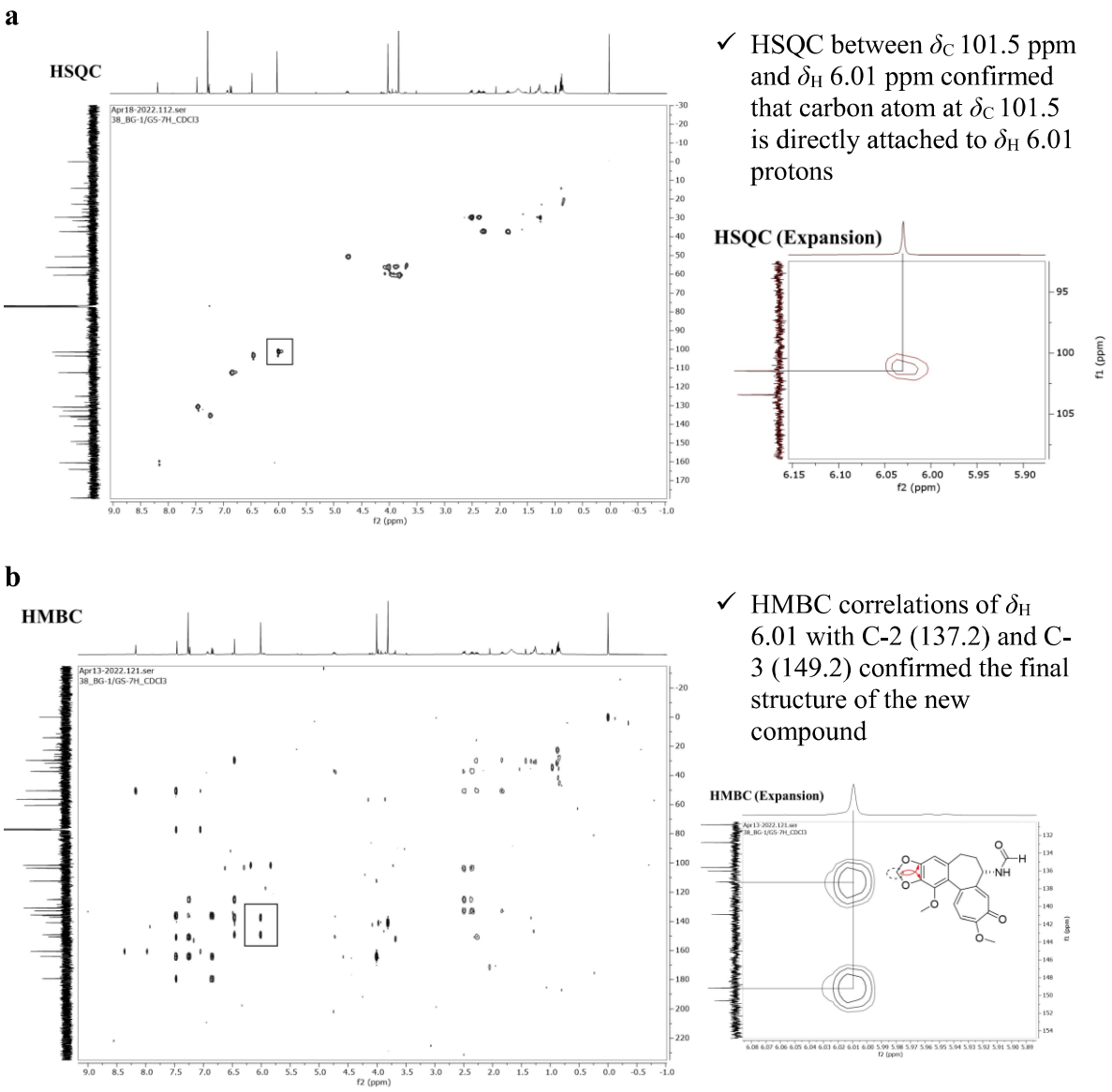

Figure 3.11. HSQC and HMBC spectra of new compound **3.19**

3.2.3. Biological activity of gloriosine

3.2.3.1. *In-vitro* cytotoxicity screening of gloriosine

Gloriosine (**3.3**) was evaluated for cytotoxic activity against a panel of fifteen human cancer cell lines of multiple tissue origin and normal breast cells, as listed in Table 3.2, using MTT assay. Colchicine (**3.2**) was used as the positive control. Surprisingly, gloriosine

exhibited highly potent activity against all the tested cancer cell lines with IC_{50} values ranging from 32 to 100 nM after 48 h, while 700 nM in the case of normal breast cells (Table 3.2). The IC_{50} values of gloriosine were less than colchicine except in some cases. Gloriosine (IC_{50}: 700 nM) appeared to be less toxic as compared to colchicine (IC_{50}: 567.8 nM) when tested in normal breast cells. Toxicity window in cancer cells and normal cells indicated that gloriosine (**3.3**) is less toxic to normal cells and more selective towards the cancer cells than colchicine (**3.2**).

Table 3.2. IC_{50} values (nM) of gloriosine (**3.3**) and colchicine (**3.2**) in various human cancer cell lines and normal cell line after 48 h

S. No.	Human Cancer Cell lines	Tissue Origin	IC_{50} ± SD (nM)	
			Gloriosine (3.3)	Colchicine (3.2)[a]
1	MCF-7	Breast	78 ± 6.23	110 ± 9.87
2	MDA-MB-231		100 ± 7.22	70 ± 9.67
3	Hs 578T		97 ± 6.99	90 ± 9.56
4	A549	Lung	35 ± 2.43	40 ± 3.32
5	NCI-H460		54 ± 3.89	64.8 ± 5.21
6	HOP-62		64 ± 4.11	86.6 ± 6.96
7	COLO 205	Colon	40 ± 2.36	120.0 ± 1.10
8	HCT 116		38 ± 2.09	140.00 ± 10.98
9	MOLT-4	Leukemia	32 ± 2.88	ND[b]
10	HL-60		45 ± 3.67	ND
11	SiHa	Cervix	78 ± 5.77	137.6 ± 12.78
12	FaDu	Oral	42 ± 3.98	ND
13	SCC-9		39 ± 3.10	ND
14	SF-295	Brain	49 ± 3.78	54.3 ± 3.499
15	U251		57 ± 4.11	76.8 ± 3.1
16	MCF-10A	Normal Breast	700 ± 27.89	567.8 ± 56.77

[a]Used as positive control.
[b]Not determined.

3.2.3.2. Nuclear staining and fluorescence microscopy

Gloriosine (**3.3**) has shown potent cytotoxicity against lung cancer cells, further experiments were performed in A549 (lung) cells. To address the cause of cell death by

gloriosine, nuclear morphological changes were studied by nuclear staining and fluorescence microscopy of A549 cells. A549 cells were treated with 50, 100, and 500 nM gloriosine (**3.3**) for 24 h. After the treatment characteristic changes of apoptosis such as the formation of apoptotic bodies, nuclear condensation, and membrane blebbing were observed in the morphology of the treated cells in a concentration-dependent manner, whereas the untreated cells' nuclei were found to have normal intact morphology. The results suggest that the gloriosine (**3.3**) was able to induce apoptotic cell morphology in A549 cells (Figure 3.12).

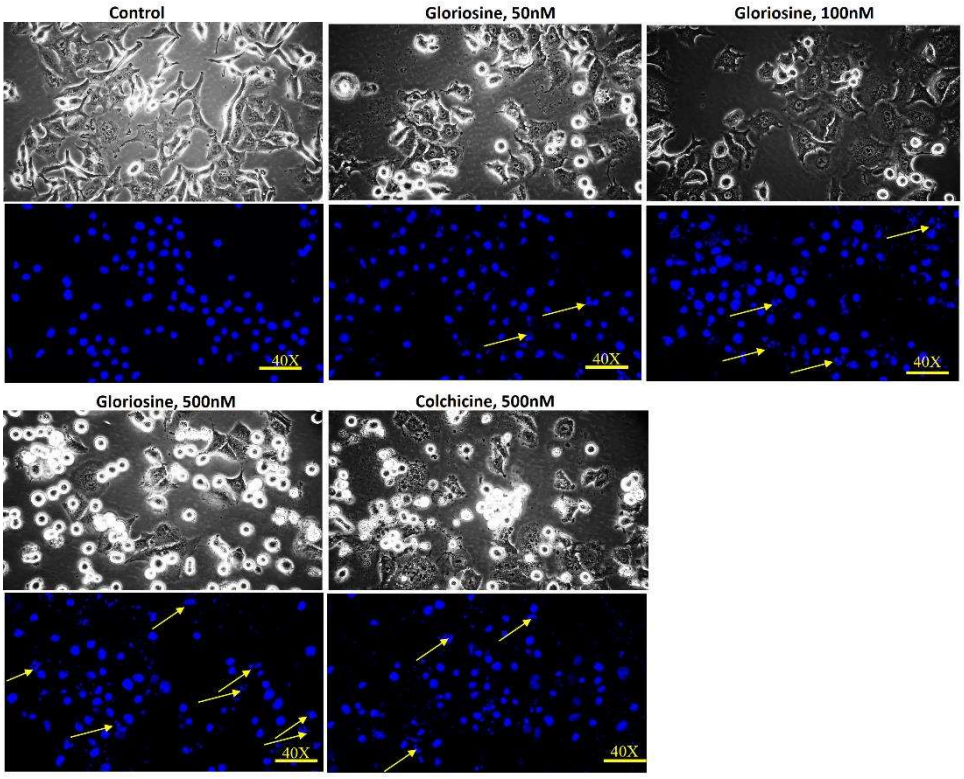

Figure 3.12. Nuclear staining after treatment with different concentrations of gloriosine (50, 100, and 500 nM) and colchicine (500 nM) on A549 cells for 24 h revealed the formation of apoptotic bodies in a dose-dependent manner.

3.2.3.3. Scratch assay for cell migration study

To assess its effect on cell migration, a wound-healing assay was performed to examine the chemotactic motility of A549 cells. At 500 nM concentration, gloriosine (**3.3**) completely inhibited the cell migration, which was more active than colchicine (Figure 3.13). Gloriosine (**3.3**) was found to greatly impede cell migration in a concentration-dependent manner. It was observed that gloriosine decreased the wound closure percentage from 85% to 11% at 500 nM concentration.

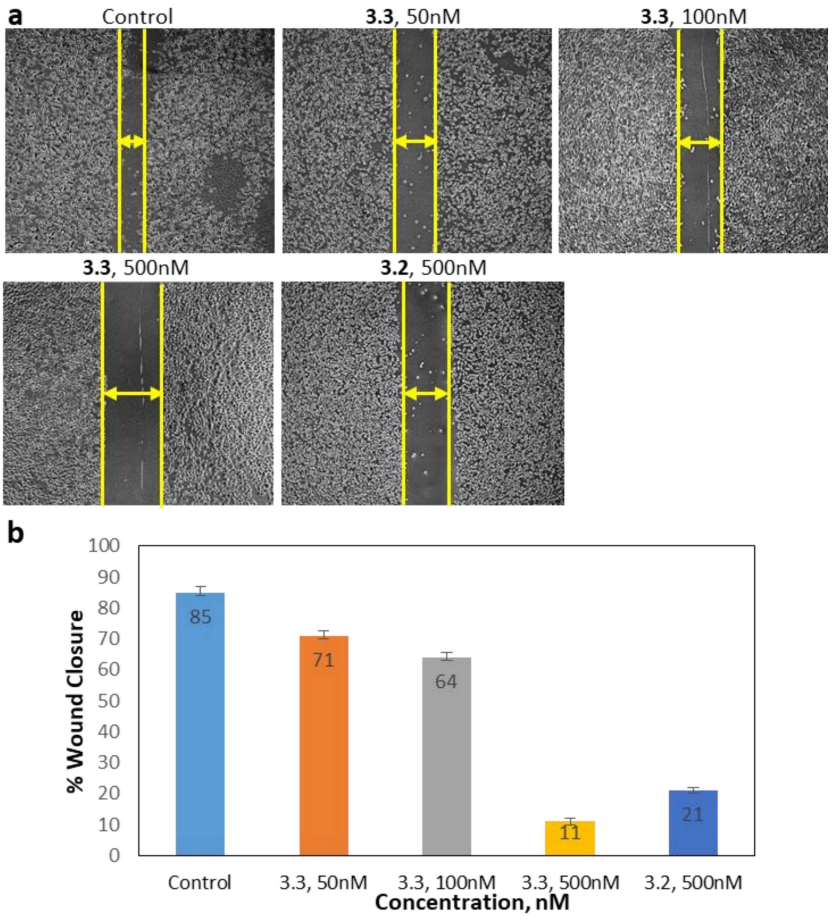

Figure 3.13. Effect of gloriosine (**3.3**) and colchicine (**3.2**) on *in-vitro* cell migration in A549 cells after 24 h. Gloriosine completely inhibited A549 cells migration at 500 nM concentration.

3.2.4. *In-silico* investigation of binding modes of gloriosine against tubulin protein

3.2.4.1. Molecular docking studies of gloriosine with tubulin protein

Since gloriosine (**3.3**) possesses all the necessary pharmacophores required for binding to the tubulin protein (as proved with colchicine), we performed the molecular docking studies of gloriosine (**3.3**) with tubulin protein (PDB:4O2B) to study the possible binding modes of colchicine-binding site. The binding energy for gloriosine (ligand) was found to be -8.06 kcal/mol for tubulin, which was almost equal to that of the colchicine (-8.01 kcal/mol). Gloriosine showed important interactions with tubulin protein such as alkyl bond with Ala180 of α-subunit, H-bond with Ala250 and Asp251 of β-subunit, and π-sigma bond with Leu255 and Leu248 of β-subunit (Figure 3.14A). The interactions of gloriosine with tubulin protein are represented in Figure 3.14. The RMSD between the co-crystallized ligand and docked ligand was found to be 0.41 Å.

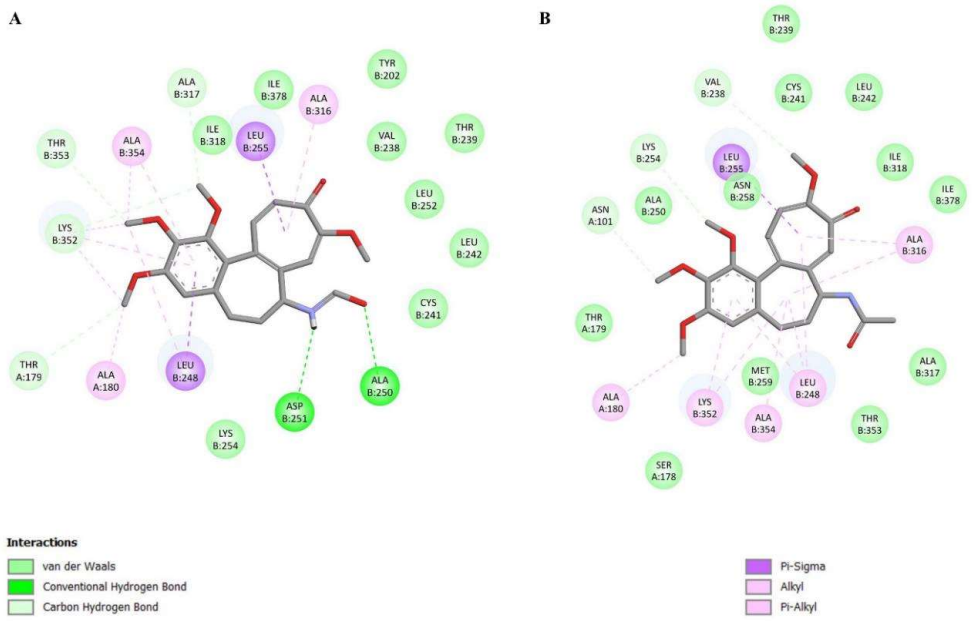

Figure 3.14. The protein-ligand interaction diagram of compounds **A)** Gloriosine and **B)** Colchicine against tubulin protein (PDB ID: 4O2B).

3.2.4.2. Molecular dynamic simulation of gloriosine with tubulin protein

MD simulation is a computational method for studying the physical movement of atoms and molecules in a biophysical system. In this study, MD simulation was done to establish the stability of the gloriosine-tubulin complex.

3.2.4.2.1. RMSD analyses

The actual movement and structural changes of a protein in a biological environment can be visualized using MD simulation. The RMSD indicates the equilibration and stability of a complex (Tripathi et al., 2022). It is evident from Figure 3.15 that protein attains a stable RMSD during the simulation run. In the case of the gloriosine-tubulin complex, the maximum protein backbone RMSD was found to be 3.42 Å which is considered perfectly fine for small and globular proteins. The average protein backbone RMSD was found to be 1.99 Å for the gloriosine-tubulin protein complex. In the same plot, it was observed that the ligands RMSD were not significantly larger than the protein RMSD which indicates that the ligand does not diffuse away from the initial binding site. The average ligand RMSD was found to be 3.04 Å for the gloriosine-tubulin protein complex.

3.2.4.2.2. RMSF analyses

The RMSF is useful for characterizing local changes along the protein chain (Mittal et al., 2021). The peaks in the plot represent the residues which fluctuates the most during simulation. The RMSF analysis was calculated for C-α atom of protein residues. The average protein RMSF was found to be 1.76 Å for gloriosine-tubulin protein complex. The residues participating in interactions with ligand i.e., Thr179, Leu255, Thr314, and Thr353 remained highly stable throughout the simulation.

3.2.4.2.3. H-bond interaction analyses

Protein interactions with the ligand were monitored throughout the simulation. The H-bond interaction analyses is important to understand the stability of predicted protein-ligand complex. H-bonding plays a significant role in accommodating the ligand inside the binding site (Pant et al., 2021). Gloriosine showed H-bond interaction with Thr179, Leu255 and Thr314. The similar interactions were also observed in docking studies as well. MD simulation study of gloriosine-tubulin complex established the stable binding of ligand with target protein.

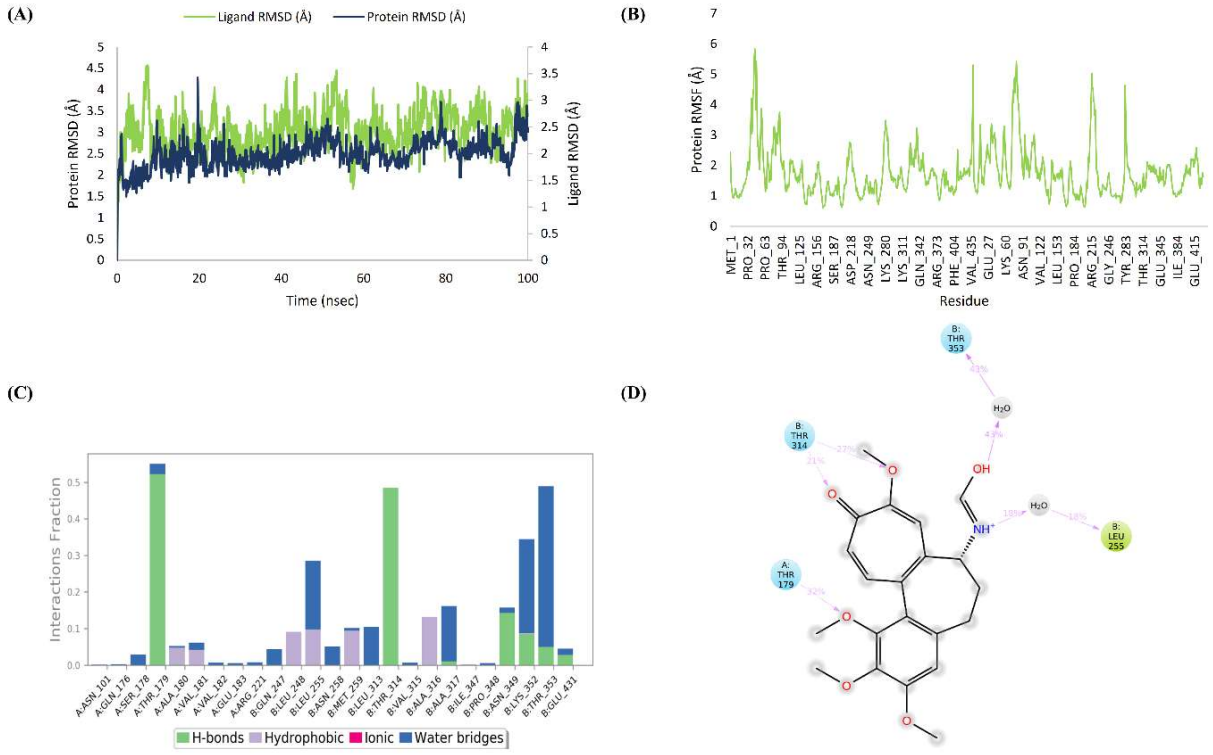

Figure 3.15. MD simulation of gloriosine complexed with tubulin. **A**. RMSD plot of tubulin and gloriosine. **B.** RMSF plot of tubulin. **C.** Protein-ligand contacts between tubulin and gloriosine during MD run. **D.** Interactions of gloriosine with tubulin during MD run.

3.2.5. Synthetic modifications of gloriosine

Gloriosine demonstrated significant cytotoxic activity in all cancer cell lines tested, with IC_{50} values ranging from 32 to 100 nM. Highest cytotoxicity was observed in MOLT4 (leukemia) cell line, with an IC_{50} of 32 nM. In several other cell lines, gloriosine was found to be more active than colchicine. Cytotoxicity of gloriosine (IC_{50} 700 nM) against normal breast cells (MCF-10A) was lower than colchicine (IC_{50} 567 nM), indicating that gloriosine may be a better option for discovering safer and more potent anticancer therapeutics.

Based on the above findings, gloriosine was identified as a potential lead for the discovery of novel compounds using a synthetic medicinal chemistry approach. Because gloriosine shared structural similarities with colchicine, we assumed that similar modifications, as reported on colchicine, would result in potent derivatives. As discussed in SAR (Figure 3.2), C-10 amino derivatives of colchicine resulted in potent compounds. Based on the above rationale, we aimed to create derivatives by modifying the C-10 position of gloriosine. We designed the following two series of gloriosine derivatives (Figure 3.16):

Series 1: C-10 amine derivatives of gloriosine

Series 2: C-10 amide derivatives of gloriosine

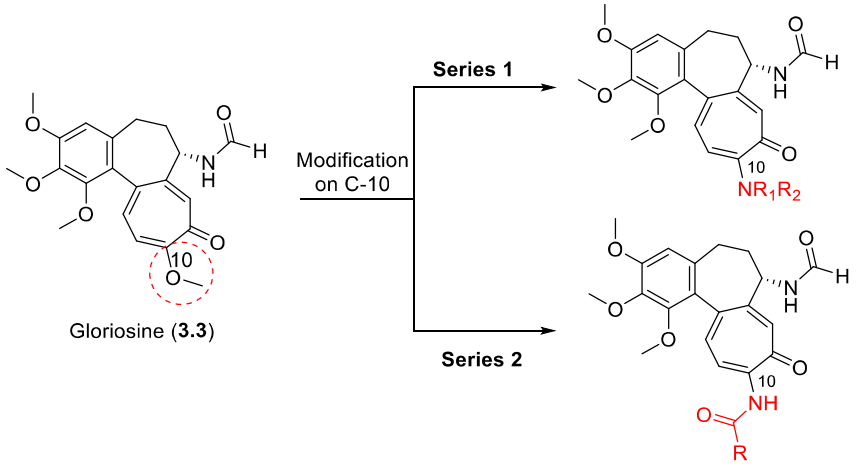

Figure 3.16. Different series of gloriosine derivatives

3.2.5.1. Series 1: Synthesis of C-10 amine derivatives of gloriosine

In gloriosine, C-10 methoxy group being adjacent to carbonyl group is most liable to nucleophillic attack by amines. A series of C-10 substituted derivatives of gloriosine were synthesized and characterized by NMR and MS analyses. Gloriosine was treated with different amines in methanol to produce the corresponding 10-amino-linked derivatives in good yields (67-95%). In general, it was noticed that amination was easier with secondary amines, as compared to substituted anilines.

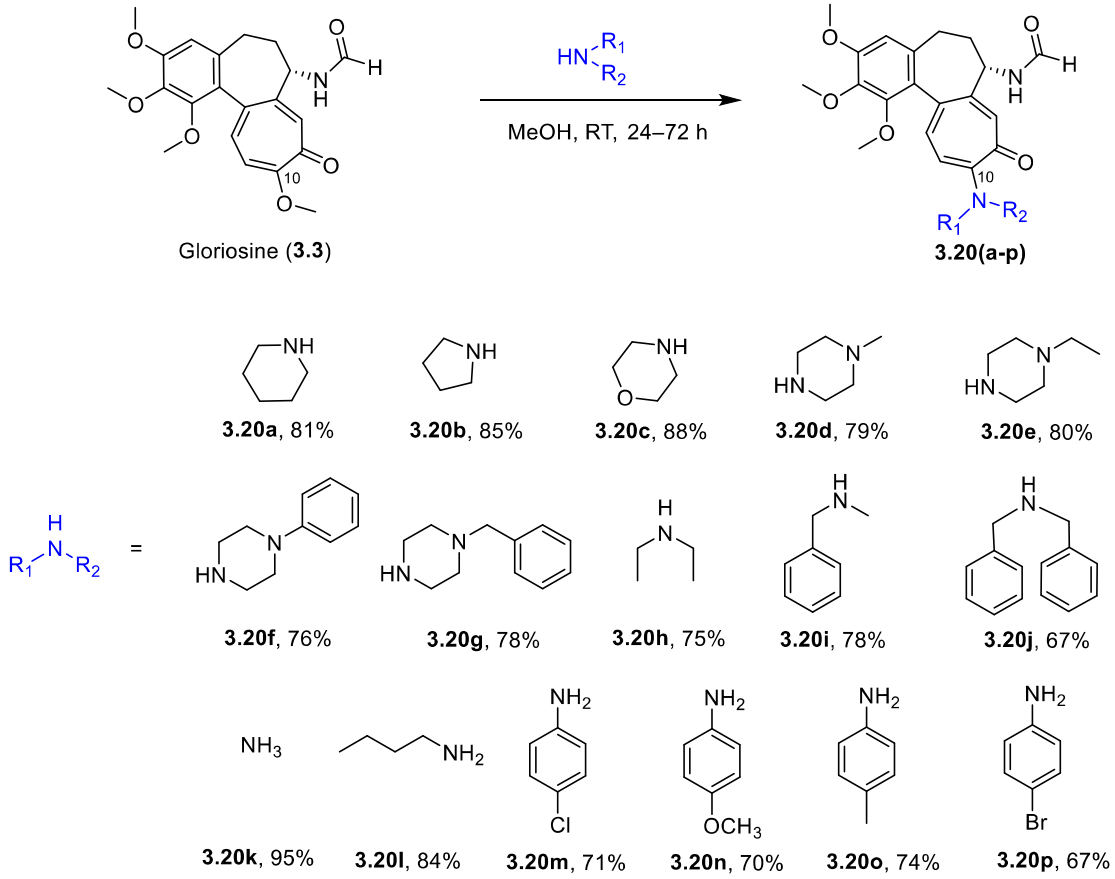

Figure 3.17. Synthesis of 10-amine derivatives of gloriosine (**3.3**). Reagents and conditions: NH-R_1R_2 (4.0 equiv.), MeOH (3 mL), rt, 24–72 h.

All synthesized compounds were purified by silica gel column and/or Sephadex LH20 column and isolated compounds were characterized based on their spectral properties. The ^{1}H NMR spectrum of synthesized derivatives showed the absence of a methoxy group at 4.1 ppm, and the corresponding carbon in ^{13}C spectrum proving the replacement of 10-OCH_3. Typical spectra of a compound from this series are represented by compound **3.20h**.

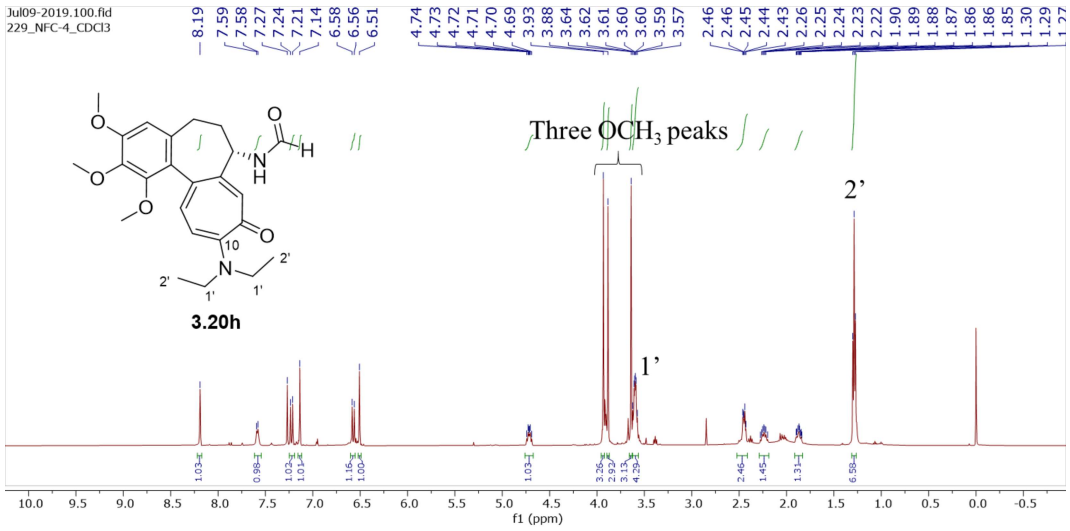

Figure 3.18. ^{1}H NMR spectrum of compound **3.20h** in $CDCl_3$ (500 MHz)

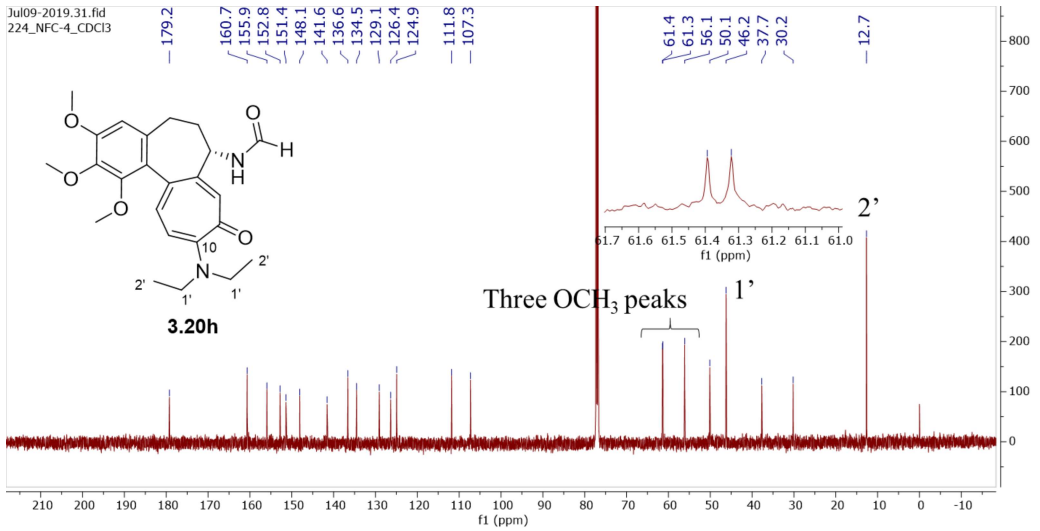

Figure 3.19. ^{13}C NMR spectrum of compound **3.20h** in $CDCl_3$ (125 MHz)

The ^{1}H and ^{13}C NMR spectra of compound **3.20h** showed the presence of only three methoxy groups, and additional peaks in the aliphatic region due to ethyl groups of diethylamine (Figures 3.18 and 3.19). In HMBC spectrum, C-10 at δ_C 155.9 ppm showed correlation with C-1' protons of amine moiety at 3.60 ppm, confirming the attachment of amine group to the C-10 (Figure 3.20).

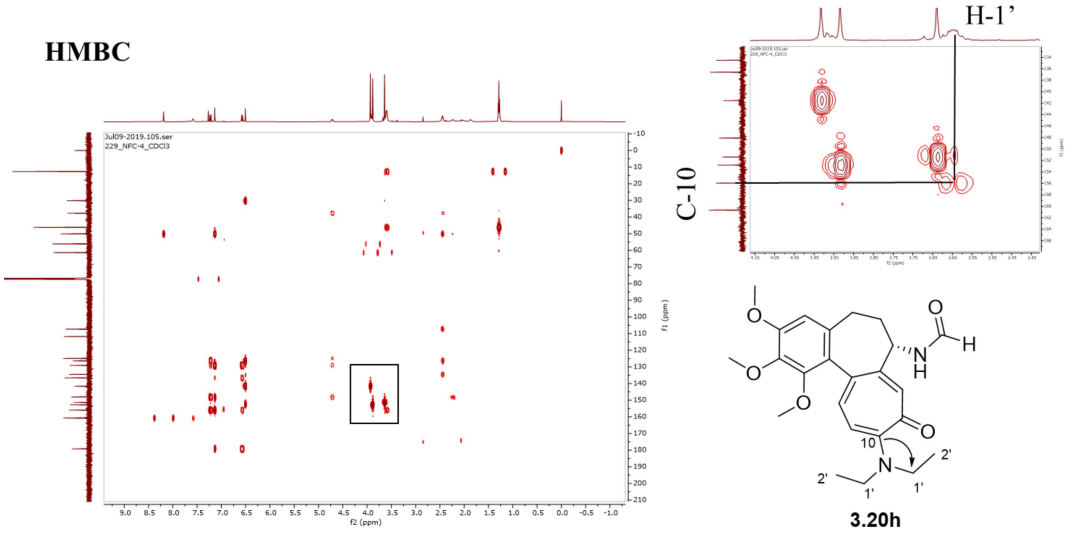

Figure 3.20. HMBC NMR spectrum of compound **3.20h**

3.2.5.2. Series 2: Synthesis of C-10 amide derivatives of gloriosine

For the synthesis of C-10 amide derivatives of gloriosine, first C-10 amino derivative of gloriosine (**3.20k**) was synthesized (as mentioned in series 1). Compound **3.20k** was then subjected to amide synthesis *via* coupling reactions like EDC/HOBt, DCC/HOBt. The amide derivative was formed in very small yield (5-10%) as observed on TLC. We could not get isolable yields after multiple attempts.

Since the quantity of gloriosine was very limited, so we initiated a model amidation reaction on colchicine (abundantly available) to optimize the reaction conditions to get isolable amount of C-10 amide derivatives.

First, the C-10 amino derivative of colchicine was synthesized using method as discussed above to synthesize 10-demethoxy-10-amino colchicine (**3.21**). Intermediate **3.21** was subjected to amidation *via* EDC and DCC coupling reactions (Figure 3.21). Desirable amide **3.22** was obtained in yield of 5-10%. The model reaction was also investigated by LCMS that confirmed the synthesis of amide derivative (Figure 3.22).

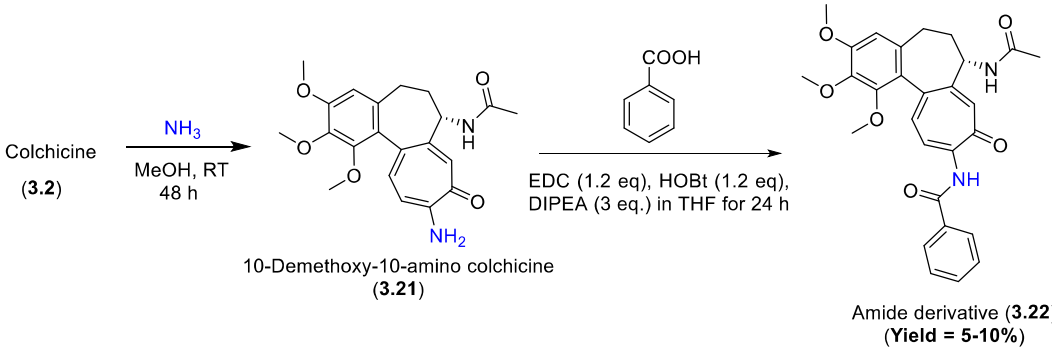

Figure 3.21. Synthesis of C-10 benzamide derivative of colchicine *via* EDC coupling reaction

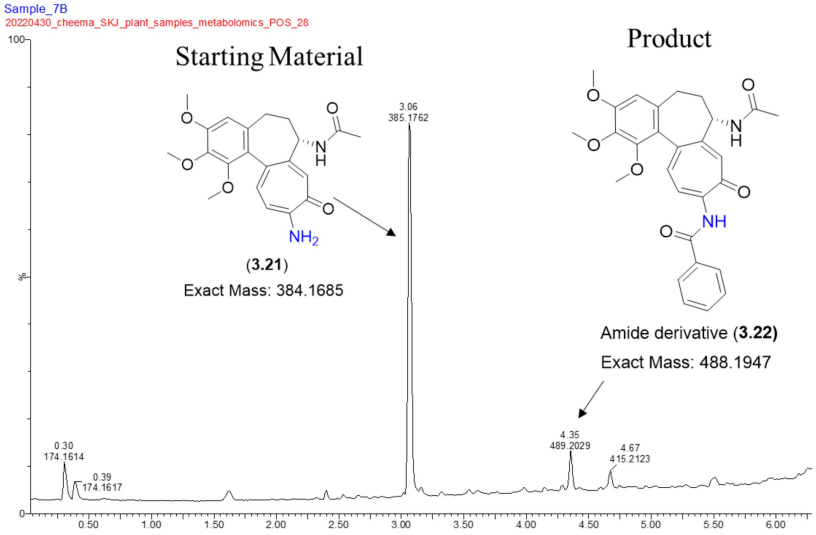

Figure 3.22. LCMS analysis of EDC coupling reaction mass. LC conditions: mobile phase A: water (0.2% formic acid) and B: acetonitrile (0.2% formic acid), elution gradient for 7 min with a flow rate of 0.4 ml/min: 0-0.5 min 0-20% B; 0.5-4 min 20-100% B; 4–5 min 100% B; 5-6 min 100-0% B and 6-7 min 0% B. The column temperature was maintained at 35 °C.

Next, we tried the amidation reaction by conventional benzoylation method. When intermediate **3.21** was subjected to react with benzoyl chloride, multiple spots were observed on TLC (monobenzoylated and dibenzoylated products) (Figure 3.23). This reaction also failed to produce an isolable yield of required amide derivatives. Similar observations have been reported previously by Singh et al. (2015).

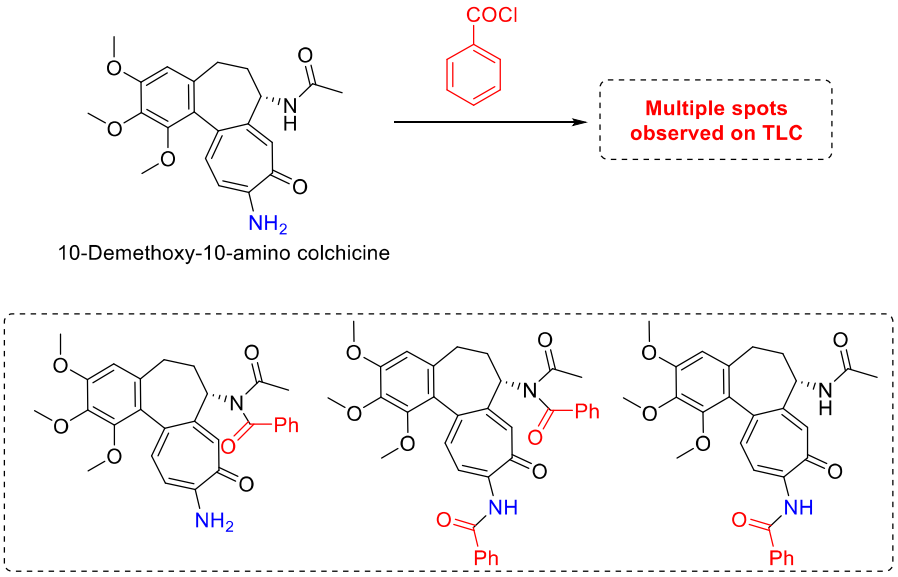

Figure 3.23. Reaction of C-10 benzamide derivative of colchicine *via* benzoylation reaction

An extensive literature search revealed that an alternative method can be planned using aldehyde as an acid equivalent to react with intermediate **3.21**. Various catalysts and protocols have been developed for amidation using amine and aldehyde. (Patel et al., 2015; Reddy et al., 2008; Gaspa et al., 2016).

Further, we initiated the development of a suitable method with metal catalyst for amidation using aldehyde (benzaldehyde) and amine (piperidine). Initially we screened many metal catalysts (Ni, Cu, Zn, $NiSO_4$, copper acetate, zinc sulphate, etc.), however the nickel catalyst was found to be good and novel among the catalysts. So, we further optimized the reaction conditions in the presence of different nickel catalysts: Ni-Ni PBA, Ni@C,

commercial NiO, NiO-Ni nanoparticles (prepared from nickel salt) and NiO@Ni (PBA derived) producing amide in 15%, 5%, 20%, 58% and 78% yield, respectively after 12 h of reaction at 100 °C (entry 3-7, Table 3.3). Addition of small amount of oxidizing agent (TBHP) drastically improved the catalytic activity to obtain optimum reaction conditions as 60 °C and 8 h.

Table 3.3. Optimization of reaction conditions. [a]

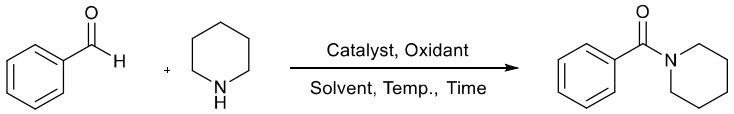

Benzaldehyde Piperidine Benzoyl piperidine

Entry	Catalyst	Oxidant	Solvent	Time (h)	Temperature (°C)	Yield (%)
Controlled reaction						
1	-	-	Dioxane	20	100	<5
2	-	TBHP (4 eq)	Dioxane	12	100	40
Catalysis without adding oxidant						
3	Ni-Ni PBA (5 mg)	-	Dioxane	12	100	15
4	Ni@C (5 mg)	-	Dioxane	12	100	<5
5	NiO (commercial) (5 mg)	-	Dioxane	12	100	20
6	NiO-Ni (5 mg)	-	Dioxane	12	100	58
7	NiO@Ni (5 mg)	-	Dioxane	12	100	78
Catalysis with oxidant						
8	NiO (commercial) (5 mg)	TBHP (4 eq)	Dioxane	8	60	52
9	NiO (5 mg)	TBHP (4 eq)	Dioxane	8	60	75
10	Ni-Ni PBA (5 mg)	TBHP (4 eq)	Dioxane	8	60	35
11	**NiO@Ni (5 mg)**	**TBHP (4 eq)**	**Dioxane**	**8**	**60**	**98**
12	NiO@Ni (5 mg)	H2O2 (4 eq)	Dioxane	8	60	85[b]
13	Ni@C (5 mg)	TBHP (4 eq)	Dioxane	8	60	30
Variation in catalyst amount						
14	NiO@Ni (1 mg)	TBHP (4 eq)	Dioxane	8	60	75
15	NiO@Ni (2 mg)	TBHP (4 eq)	Dioxane	8	60	75
16	NiO@Ni (3 mg)	TBHP (4 eq)	Dioxane	8	60	78
17	NiO@Ni (4 mg)	TBHP (4 eq)	Dioxane	8	60	80
18	NiO@Ni (10 mg)	TBHP (4 eq)	Dioxane	8	60	95
19	NiO@Ni (15 mg)	TBHP (4 eq)	Dioxane	8	60	95
Variation in TBHP amount						
20	NiO@Ni (5 mg)	TBHP (1eq)	Dioxane	8	60	72
21	NiO@Ni (5 mg)	TBHP (2 eq)	Dioxane	8	60	78
22	NiO@Ni (5 mg)	TBHP (8 eq)	Dioxane	8	60	96
Variation of solvent						
23	NiO@Ni (5 mg)	TBHP (4 eq)	DMF	8	60	50
24	NiO@Ni (5 mg)	TBHP (4 eq)	THF	8	60	80
25	NiO@Ni (5 mg)	TBHP (4 eq)	Water	8	60	10$
26	NiO@Ni (5 mg)	TBHP (4 eq)	MeOH	8	60	30$
Effect of nitrogen atmosphere						
27	NiO@Ni (5 mg)	TBHP (4 eq)	Dioxane	8	60	36 [c]

[a]Under nitrogen atmosphere. [b]Acid and ester was observed as the major product instead of amide. [c]Under atomospheric condition (without nitrogen atmosphere), $acid was observed as major product.

The amount of catalyst also played an important role in the reaction process. 5 mg NiO@Ni was found to be an optimum amount of catalyst for 1 mmol of each reactant (Entry 11, Table 3.3). A significant effect of the solvents on reaction yield and product selectivity was observed. Aprotic solvents produced better yield. The order of yield for amidation was as follows: dioxane>THF>DMF (Entry 11, 23–24, Table 3.3). In the absence of nitrogen atmosphere, lower yield of the amide was obtained (Entry 27, Table 3.3).

Table 3.4. Scope of the amidation reaction.

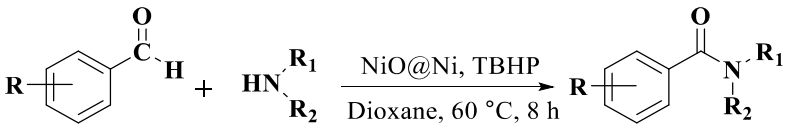

3.23 **3.24** **3.25**

Entry	R	R_1R_2NH	Product	Yield (%)
1	H	Piperidine	**3.25a**	98
2	4-OCH_3	Piperidine	**3.25b**	92
3	3-Br	Piperidine	**3.25c**	95
4	4-Cl	Piperidine	**3.25d**	96
5	2-OH	Piperidine	**3.25e**	70
6	2-NO_2	Piperidine	**3.25f**	88
7	4-NO_2	Piperidine	**3.25g**	92
8	4-Cl	Morpholine	**3.25h**	98
9	4-Cl	Pyrrolidine	**3.25i**	90
10	3-Br	Pyrrolidine	**3.25j**	89
11	4-Cl	N-Me benzyl amine	**3.25k**	90
12	3-Br	Morpholine	**3.25l**	90
13	3-Br	Diethyl amine	**3.25m**	91
14	4-Cl	Benzyl amine	**3.25n**	92
15	H	Benzyl amine	**3.25o**	92
16	3-Br	Benzyl amine	**3.25p**	90
17	4-NO_2	Benzyl amine	**3.25q**	85
18	4-Cl	n-Butyl amine	**3.25r**	75
19	H	Valine methyl ester	**3.25s**	94
20	4-Cl	Valine methyl ester	**3.25t**	94
21	H	leucine methyl ester	**3.25u**	98

Then the scope of the reaction was explored taking different substituted benzaldehydes and different primary and secondary amines. To generalize the scope of the amide bond formation, the reaction was further extended to synthesize the peptides of amino acids. Amino acid methyl esters gave corresponding amides in excellent yield.

A tentative mechanism was proposed for the NiO@Ni catalyzed oxidative amination of benzaldehydes. The reaction proceeds through a radical mechanism, as discussed earlier (Subhedar et al., 2018). First, NiO@Ni catalyzed the homolytic cleavage of TBHP to form $^{t}BuO^{\bullet}$ and $OH^{\bullet}$ radicals. Adsorption of substrates (amine and benzaldehyde) on catalyst surface facilitates the formation of corresponding radicals by reacting with $^{t}BuO^{\bullet}$ and/or $OH^{\bullet}$ radicals. At last, the radical-radical coupling of acyl and amine radical takes place, resulting in the amide bond formation. Furthermore, the method was utilized to synthesize the C-10 amide derivatives of colchicine and gloriosine.

To check the application of the developed method, the intermediate 10-demethoxy-10-aminocolchicine (**3.21**) and benzaldehyde were subjected to amidation under the optimized reaction condition. To our surprise, the yield of desirable product was improved to 62% as analyzed by LCMS (Figures 3.24 & 3.25)

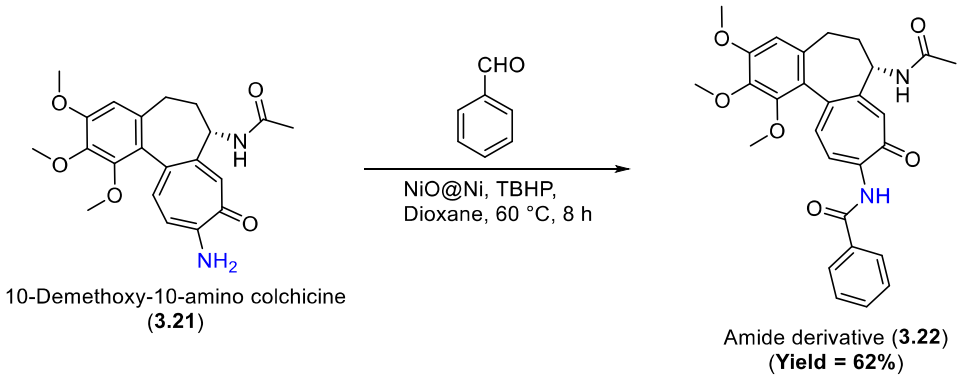

Figure 3.24. Synthesis of C-10 amide derivative of colchicine via oxidative amidation reaction

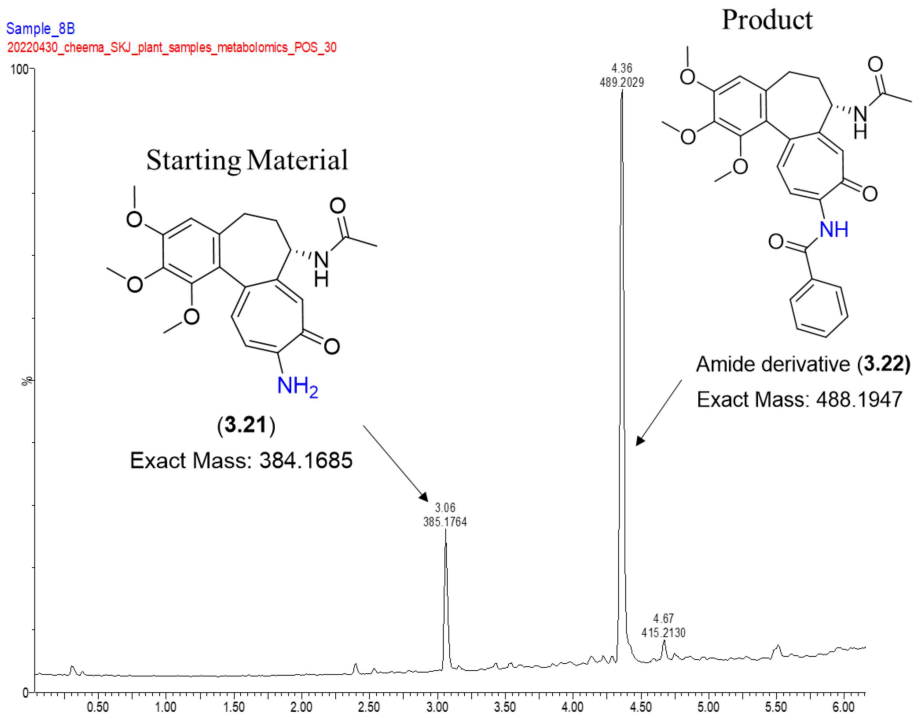

Figure 3.25. LCMS analysis of oxidative amidation reaction mass

Although we attempted to optimize the reaction further in order to obtain a higher yield of C-10 amide derivative **3.22**, but we couldn't get the better yield. Since, it produced an isolable amount of desired amide derivatives, we used this method for the synthesis of more C-10 amide derivatives of gloriosine. The yield of different derivatives varied between 45-62%. It is noteworthy to mention, that some uncharacterized impurities were generated during the reaction.

Due to the limited quantity of gloriosine and moderate product yield, only four amide derivatives were synthesized (Figure 3.26). The amide bond formation was confirmed by the NMR spectroscopy. The typical spectrum is represented by compound **3.26a**, in which a new peak due to carbonyl group of amide appeared at 170.11 ppm (Figure 3.27). The synthesized derivatives **3.26**(**a-d**) were characterized based on their spectral properties.

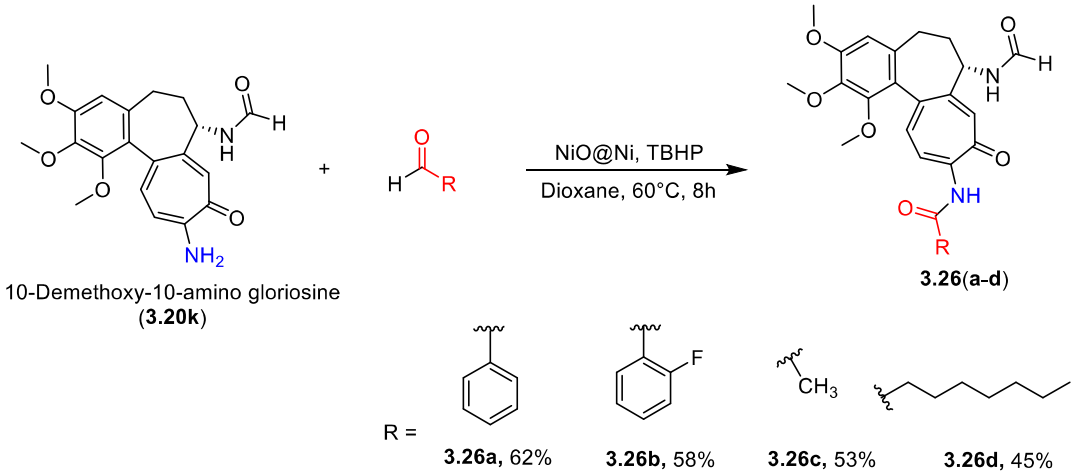

Figure 3.26. Synthesis of C-10 amide derivatives of gloriosine

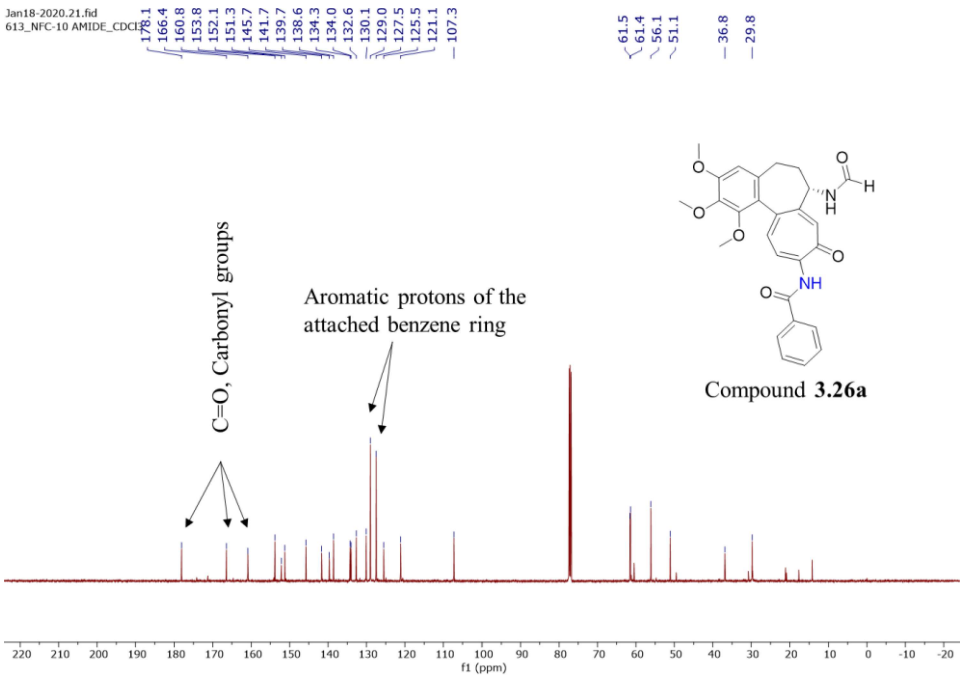

Figure 3.27. ^{13}C NMR spectrum of compound **3.26a** in $CDCl_3$ (125 MHz)

3.3. Experimental section

3.3.1. General experimental procedures

All the chemicals were obtained from Sigma-Aldrich company and used as received. The ^{1}H and ^{13}C NMR spectra were recorded on Bruker-Avance III HD 500 MHz and 125

MHz NMR instruments respectively. Chemical shifts are reported in parts per million (ppm) downfield from tetramethylsilane (TMS) and are referenced to the residual proton/carbon in the NMR solvent ($CDCl_3$, 7.26/77.1 ppm; MeOD, 3.31/49.00 ppm; DMSO-d_6, 2.50/39.5 ppm). The Acquity UPLC (Waters Corporation, USA) and MS (Xevo G2S, qToF) system was used for LCMS. The samples were resolved on an Acquity UPLC BEH C-18, 1.7μM, 2.1 mm X 50 mm column. All chromatographic purifications were performed on silica gel (#60−120 or #100−200) obtained from Merck. The thin-layer chromatography (TLC) was performed on pre-coated silica gel 60 GF254 aluminum sheets (Merck) and visualized under UV light (254 nm) and by spraying anisaldehyde−sulfuric acid reagent followed by heating.

3.3.2. Plant material

The dried roots and tubers of *Gloriosa superba* were purchased from the local market of Varanasi, India, in January 2020 and authenticated by Dr. Bikarma Singh, Senior Scientist at CSIR-IIIM Jammu. A specimen sample (accession number: RRLH57502) was preserved in Janaki Ammal Herbarium at the CSIR-IIIM, Jammu, India.

3.3.3. Extraction and isolation

The dried roots of *G. superba* (2 kg) were coarsely powdered and extracted three times (4 L, each) with chloroform: methanol (v/v, 1:1) at room temperature. The crude extract was filtered and evaporated to dryness *in vacuo* to yield 163 g of semisolid material. The dried extract was chromatographed over silica gel (#100-200) and eluted with *n*-hexane-ethyl acetate step gradient system (v/v, 1:0 → 0:1) and then with ethyl acetate : methanol (v/v, 1:0 → 9:1). First, the extract was defatted with hexane. With an increasing percentage of ethyl acetate (5 %), stigmasterol and *β*-sitosterol were obtained. Further increasing the percentage of ethyl acetate in a step-gradient manner afforded trioxsalen, caffeic acid, 6-methoxy

salicylic acid, *β*-lumicolchicine, N-deacetyl-N-formyl-*β*-lumicolchicine, 2-demethyl-*β*-lumicolchicine, *γ*-lumicolchicine, colchicine, gloriosine, 3-demethylcolchicine, 3-demethyl-N-deacetyl-N-formyl colchicine, and colchicoside. All the compounds were purified by repeated silica gel column chromatography.

6-Methoxy salicylic acid (3.1): See Appendix (Kühnert and Maier, 2002).

Colchicine (3.2): 1.8 gm; ^{1}H NMR (500 MHz, $CDCl_3$) δ 8.10 (d, *J* = 6.5 Hz, 1H), 7.61 (s, 1H), 7.36 (d, *J* = 10.7 Hz, 1H), 6.90 (d, *J* = 10.8 Hz, 1H), 6.55 (s, 1H), 4.66 (dt, *J* = 11.8, 6.2 Hz, 1H), 4.02 (s, 3H), 3.95 (s, 3H), 3.92 (s, 3H), 3.67 (s, 3H), 2.53 (dd, *J* = 12.9, 5.6 Hz, 1H), 2.45 – 2.28 (m, 2H), 1.97 (s, 3H), 1.96 – 1.95 (m, 1H). ^{13}C NMR (125 MHz, $CDCl_3$) δ 179.5, 170.1, 164.0, 153.6, 152.5, 151.2, 141.7, 137.0, 135.6, 134.3, 130.5, 125.6, 112.9, 107.4, 61.6, 61.4, 56.4, 56.1, 52.7, 36.4, 29.9, 22.8 (Alali et al., 2005).

Gloriosine (3.3): 1.1 gm; ^{1}H NMR (500 MHz, $CDCl_3$) δ 8.25 (dd, 1H), 8.18 (s, 1H), 7.61 (s, 1H), 7.36 (d, *J* = 10.6 Hz, 1H), 6.91 (d, *J* = 10.9 Hz, 1H), 6.55 (d, *J* = 1.7 Hz, 1H), 4.73 (p, *J* = 6.4 Hz, 1H), 4.02 (s, 3H), 3.95 (s, 3H), 3.92 (s, 3H), 3.66 (s, 3H), 2.54 (m, 1H), 2.46 – 2.29 (m, 2H), 1.98 (m, 1H). ^{13}C NMR (125 MHz, $CDCl_3$) δ 179.5, 164.1, 160.9, 153.6, 151.3, 151.2, 141.7, 136.6, 135.6, 134.1, 130.8, 125.5, 112.8, 107.3, 61.6, 61.4, 56.5, 56.1, 51.1, 36.7, 29.8 (Capraro and Brossi, 1984).

3-Demethylcolchicine (3.4): 45 mg; ^{1}H NMR (500 MHz, $CDCl_3$) δ 8.44 (d, *J* = 6.3 Hz, 1H), 7.65 (s, 1H), 7.36 (d, *J* = 10.7 Hz, 1H), 6.92 (d, *J* = 11.0 Hz, 1H), 6.56 (s, 1H), 4.64 (dt, *J* = 11.9, 5.9 Hz, 1H), 4.00 (s, 3H), 3.97 (s, 3H), 3.63 (s, 3H), 2.44 (d, *J* = 7.4 Hz, 1H), 2.35 – 2.23 (m, 2H), 1.97 (s, 3H), 1.95 – 1.87 (m, 1H). ^{13}C NMR (125 MHz, $CDCl_3$) δ 179.6, 170.5, 164.0, 153.0, 150.3, 150.1, 139.3, 137.3, 135.7, 134.7, 130.4, 124.7, 113.2, 110.4, 61.4, 61.3, 56.4, 52.9, 36.2, 29.5, 22.6 (Alali et al., 2005).

3-Demethylgloriosine (3.5): 39 mg; ^{1}H NMR (500 MHz, $CDCl_3$) δ 8.17 (s, 1H), 8.16 – 8.04 (m, 1H), 7.60 (s, 1H), 7.35 (d, *J* = 10.7 Hz, 1H), 6.91 (d, *J* = 10.9 Hz, 1H), 6.59 (s, 1H), 4.72 (dt, *J* = 11.5, 6.2 Hz, 1H), 4.02 (s, 3H), 4.00 (s, 3H), 3.64 (s, 3H), 2.49 (m, 1H), 2.31 (m, 2H), 1.93 (m, 1H). ^{13}C NMR (125 MHz, $CDCl_3$) δ 179.6, 164.0, 161.1, 151.7, 150.2, 149.9, 139.2, 136.8, 135.6, 134.6, 130.7, 124.7, 113.0, 110.4, 61.4, 61.3, 56.5, 51.2, 36.5, 29.4 (Capraro and Brossi, 1984).

***β*-Lumicolchicine (3.10):** 9 mg; ^{1}H NMR (500 MHz, $CDCl_3$) δ 6.68 (d, *J* = 3.3 Hz, 1H), 6.49 (s, 1H), 6.04 (d, *J* = 7.2 Hz, 1H), 4.82 (m, 1H), 4.12 (q, *J* = 3.0 Hz, 1H), 3.97 (s, 3H), 3.88 (s, 3H), 3.86 (s, 3H), 3.71 (s, 3H), 3.63 (dd, *J* = 2.8, 1.7 Hz, 1H), 2.77 (dd, *J* = 15.4, 9.2 Hz, 1H), 2.58 (dd, *J* = 15.5, 9.6 Hz, 1H), 2.07 (s, 3H), 2.07 – 1.99 (m, 1H), 2.00 – 1.91 (m, 1H). ^{13}C NMR (125 MHz, $CDCl_3$) δ 201.0, 170.4, 157.8, 153.1, 151.8, 145.2, 140.3, 138.8, 137.3, 128.9, 117.7, 109.2, 61.4, 60.9, 56.9, 56.0, 51.5, 43.2, 32.6, 31.3, 23.5 (Meksuriyen et al., 1988).

2-Demethyl-*β*-lumicolchicine (3.11): 8 mg; ^{1}H NMR (500 MHz, $CDCl_3$) δ 6.73 (d, *J* = 3.2 Hz, 1H), 6.49 (s, 1H), 6.01 (d, *J* = 7.1 Hz, 1H), 5.50 (s, 1H), 4.84 (m, 1H), 4.15 (q, *J* = 3.0 Hz, 1H), 3.98 (s, 3H), 3.91 (s, 3H), 3.71 (s, 3H), 3.66 (dd, *J* = 2.8, 1.8 Hz, 1H), 2.78 (dd, *J* = 15.5, 9.0 Hz, 1H), 2.57 (dd, *J* = 15.5, 9.4 Hz, 1H), 2.09 (s, 3H), 2.06 – 1.94 (m, 2H). ^{13}C NMR (125 MHz, $CDCl_3$) δ 201.0, 170.3, 157.8, 147.0, 145.3, 145.2, 137.5, 136.7, 134.6, 129.1, 117.9, 108.1, 61.1, 56.9, 56.2, 51.5, 51.5, 43.2, 32.4, 31.5, 23.6 (Meksuriyen et al., 1988).

Colchicoside (3.12): 15 mg; ^{1}H NMR (500 MHz, MeOD) δ 7.43 (d, *J* = 10.7 Hz, 1H), 7.40 (s, 1H), 7.22 (d, *J* = 11.0 Hz, 1H), 6.93 (s, 1H), 5.03 (d, *J* = 7.6 Hz, 1H), 4.50 (dd, *J* = 11.9, 6.4 Hz, 1H), 4.02 (s, 3H), 3.96 (s, 3H), 3.94 (dd, *J* = 12.1, 2.3 Hz, 1H), 3.70 (dd, *J* = 12.1,

6.4 Hz, 1H), 3.62 (s, 3H), 3.56 (dd, *J* = 9.2, 7.6 Hz, 1H), 3.53 – 3.48 (m, 2H), 3.43 – 3.35 (m, 1H), 2.64 (dd, *J* = 13.2, 6.1 Hz, 1H), 2.32 (dt, *J* = 13.0, 6.5 Hz, 1H), 2.23 (dt, *J* = 12.7, 6.2 Hz, 1H), 2.01 (s, 3H), 1.97 – 1.87 (m, 1H). ^{13}C NMR (125 MHz, MeOD) δ 179.5, 171.3, 164.1, 152.9, 151.3, 150.9, 141.9, 137.0, 136.4, 134.6, 129.7, 127.1, 113.6, 111.4, 100.8, 77.0, 76.8, 73.5, 70.1, 61.3, 60.7, 60.5, 55.6, 52.4, 35.7, 29.0, 21.0 (Zarev et al., 2017).

Trioxsalen (3.13): 10mg; ^{1}H NMR (500 MHz, $CDCl_3$) δ 7.53 (s, 1H), 6.43 (d, *J* = 1.2 Hz, 1H), 6.25 (d, *J* = 1.3 Hz, 1H), 2.60 (s, 3H), 2.51 (d, *J* = 1.1 Hz, 3H), 2.50 (d, *J* = 1.2 Hz, 3H). ^{13}C NMR (125 MHz, $CDCl_3$) δ 161.6, 157.4, 155.5, 153.2, 148.9, 125.4, 116.1, 112.8, 112.2, 109.1, 102.6, 19.3, 14.2, 8.6 (Hassan and Loutfy, 1981).

Caffeic acid (3.14): See Appendix (Morishita et al., 1984).

***N*-Deacetyl-*N*-formyl-*β*-lumicolchicine (3.15):** 11 mg; ^{1}H NMR (500 MHz, $CDCl_3$) δ 8.22 (s, 1H), 6.68 (d, *J* = 3.2 Hz, 1H), 6.51 (s, 1H), 6.22 (s, 1H), 4.93 (d, *J* = 6.4 Hz, 1H), 4.20 – 4.10 (m, 1H), 3.99 (s, 3H), 3.90 (s, 3H), 3.88 (s, 3H), 3.68 (s, 3H), 3.67 – 3.59 (m, 1H), 2.84 – 2.70 (m, 1H), 2.62 (ddd, *J* = 15.3, 9.0, 1.7 Hz, 1H), 2.13 – 1.97 (m, 2H). ^{13}C NMR (125 MHz, $CDCl_3$) δ 200.8, 161.2, 157.7, 153.3, 151.8, 145.9, 140.4, 138.8, 136.6, 128.8, 117.6, 109.2, 61.4, 60.9, 56.8, 56.0, 51.5, 50.2, 43.2, 32.4, 31.2 (Canonica et al., 1967).

3-Demethyl-*β*-lumicolchicine (3.16): 10 mg; ^{1}H NMR (500 MHz, $CDCl_3$) δ 6.67 (d, *J* = 3.2 Hz, 1H), 6.56 (s, 1H), 5.94 (d, *J* = 7.2 Hz, 1H), 4.93 – 4.78 (m, 1H), 4.12 (q, *J* = 2.9 Hz, 1H), 3.97 (s, 3H), 3.94 (s, 3H), 3.74 (s, 3H), 3.65 (dd, *J* = 2.8, 1.8 Hz, 1H), 2.74 (dd, *J* = 15.3, 9.4 Hz, 1H), 2.55 (dd, *J* = 15.5, 9.7 Hz, 1H), 2.08 (s, 3H), 2.03 (dd, *J* = 8.9, 5.0 Hz, 1H), 1.99 – 1.90 (m, 1H). ^{13}C NMR (125 MHz, $CDCl_3$) δ 200.9, 170.4, 157.9, 150.9, 149.4, 145.0, 139.6, 138.0, 137.2, 128.6, 117.4, 112.3, 60.8, 60.8, 56.9, 51.4, 43.1, 32.2, 31.3, 23.6 (Alali et al., 2005).

3-Demethyl-*N*-Deacetyl-*N*-formyl-*β*-lumicolchicine (3.17): 8 mg; ^{1}H NMR (500 MHz, $CDCl_3$) δ 8.22 (s, 1H), 6.66 (d, *J* = 3.2 Hz, 1H), 6.57 (s, 1H), 6.11 (d, *J* = 6.9 Hz, 1H), 4.93 (d, *J* = 6.1 Hz, 1H), 4.13 (q, *J* = 2.9 Hz, 1H), 3.97 (s, 3H), 3.94 (s, 3H), 3.72 (s, 3H), 3.66 (dd, *J* = 2.9, 1.7 Hz, 1H), 2.75 (dd, *J* = 15.0, 8.2 Hz, 1H), 2.57 (dd, *J* = 14.8, 9.8 Hz, 1H), 2.11 – 1.97 (m, 2H). ^{13}C NMR (125 MHz, $CDCl_3$) δ 200.7, 161.2, 157.8, 151.0, 149.6, 145.8, 139.6, 138.0, 136.4, 128.6, 117.3, 112.4, 60.8, 60.8, 56.8, 51.4, 50.1, 43.1, 32.0, 31.2 (Al-Tel et al., 1991).

***γ*-Lumicolchicine (3.18):** 9 mg; ^{1}H NMR (500 MHz, $CDCl_3$) δ 6.63 (d, *J* = 3.3 Hz, 1H), 6.50 (s, 1H), 5.68 (d, *J* = 7.7 Hz, 1H), 4.74 – 4.65 (m, 1H), 4.07 (m, 1H), 3.98 (s, 3H), 3.89 (s, 3H), 3.88 (s, 3H), 3.71 (s, 3H), 3.63 (dd, *J* = 2.8, 1.3 Hz, 1H), 2.75 – 2.62 (m, 2H), 2.11 – 2.06 (m, 1H), 2.05 (s, 3H), 2.00 (m, 1H). ^{13}C NMR (125 MHz, $CDCl_3$) δ 198.6, 169.2, 157.3, 153.2, 151.9, 146.8, 140.3, 138.9, 138.5, 127.7, 117.8, 109.2, 61.4, 60.9, 56.8, 56.0, 50.2, 49.3, 43.1, 32.3, 30.8, 23.6 (Meksuriyen et al., 1988).

Glorigerine; *N*-deacetyl-*N*-formylcornigerine (3.19): 6 mg; ^{1}H NMR (500 MHz, $CDCl_3$) δ 8.17 (s, 1H), 7.46 (s, 1H), 7.25 (d, *J* = 10.7 Hz, 1H), 6.93 (d, *J* = 7.5 Hz, 1H), 6.85 (d, *J* = 10.9 Hz, 1H), 6.46 (s, 1H), 6.01 (s, 2H), 4.74 (dt, *J* = 12.1, 6.9 Hz, 1H), 4.01 (s, 3H), 3.81 (s, 3H), 2.50 (m, 1H), 2.36 (m, 1H), 2.27 (m, 1H), 1.87 – 1.78 (m, 1H). ^{13}C NMR (125 MHz, $CDCl_3$) δ 179.4, 164.1, 160.5, 150.6, 149.2, 140.9, 137.2, 136.0, 135.6, 132.8, 130.8, 125.1, 112.4, 103.4, 101.5, 60.6, 56.4, 50.6, 37.3, 29.7. HRMS *m/z* 370.1282 $[M + H]^+$ (calcd for $C_{20}H_{20}NO_6^+$, 370.1285).

3.3.4. Synthetic modifications on gloriosine and new synthetic method

3.3.4.1. Synthesis of C-10 amine derivatives of gloriosine

To a solution of gloriosine (96 mg, 0.25 mmol) in 3 ml of methanol, corresponding amines (1.0 mmol) were added. The reaction mixture was stirred at room temperature for 24 h-72 h. The reaction was monitored for completion by thin-layer chromatography. After completion, the reaction mixture was evaporated to dryness under vacuum, and partitioned between cold water and ethyl acetate. The organic layer was dried over anhydrous sodium sulfate and concentrated under vacuum. The crude product was purified with silica gel column chromatography and Sephadex gel filtration to get pure compounds **4.20(a-p)**.

(*S*)-*N*-(1,2,3-trimethoxy-9-oxo-10-(piperidin-1-yl)-5,6,7,9-tetrahydrobenzo[a]heptalen-7-yl)formamide (3.20a): Yellow solid; ^{1}H NMR ($CDCl_3$, 500 MHz): δ 8.19 (s, 1H), 8.14 (d, *J* = 7.6 Hz, 1H), 7.35 (s, 1H), 7.24 (d, *J* = 11.1 Hz, 1H), 6.79 (d, *J* = 11.2 Hz, 1H), 6.52 (s, 1H), 4.80 – 4.68 (m, 1H), 3.93 (s, 3H), 3.89 (s, 3H), 3.65 (s, 3H), 3.51 (d, *J* = 11.9 Hz, 2H), 3.39 (d, *J* = 7.1 Hz, 2H), 2.53 – 2.35 (m, 2H), 2.29 – 2.18 (m, 1H), 1.92 (td, *J* = 11.9, 6.9 Hz, 1H), 1.83 – 1.64 (m, 6H); ^{13}C NMR ($CDCl_3$, 125 MHz): δ 181.2, 160.9, 158.8, 153.1, 151.3, 148.9, 141.5, 136.4, 134.4, 132.9, 128.6, 126.1, 117.6, 107.3, 61.4, 61.4, 56.1, 50.3, 50.2, 37.1, 30.1, 26.0, 24.6; ESIMS *m/z* 439.30 $[M+H]^+$ (calcd for $C_{25}H_{31}N_2O_5^+$, 439.22).

(*S*)-*N*-(1,2,3-trimethoxy-9-oxo-10-(pyrrolidin-1-yl)-5,6,7,9-tetrahydrobenzo-[a]heptalen-7-yl)formamide (3.20b): Yellow solid; ^{1}H NMR (500 MHz, $CDCl_3$): δ 8.22 (s, 1H), 8.03 (d, *J* = 7.5 Hz, 1H), 7.25 (d, *J* = 11.3 Hz, 1H), 7.21 (s, 1H), 6.51 (s, 1H), 6.41 (d, *J* = 11.4 Hz, 1H), 4.70 (dt, *J* = 13.9, 7.1 Hz, 1H), 3.95 (s, 3H), 3.89 (s, 3H), 3.65 (s, 3H), 3.57 (d, *J* = 4.3 Hz, 2H), 2.45 (dd, *J* = 10.4, 4.6 Hz, 2H), 2.23 (dt, *J* = 16.5, 10.7 Hz, 1H), 2.10 – 2.00 (m, 3H), 1.99 – 1.90 (m, 4H), 1.90 – 1.84 (m, 1H). ^{13}C NMR (125 MHz, $CDCl_3$): δ

178.3, 160.9, 155.4, 152.7, 151.4, 149.0, 141.5, 137.3, 134.5, 128.2, 126.6, 124.7, 111.3, 107.3, 61.4, 61.3, 56.1, 50.8, 50.4, 37.6, 30.2, 25.4; ESIMS *m/z* 425.30 $[M+H]^+$ (calcd for $C_{24}H_{29}N_2O_5^+$, 425.21)

(*S*)-*N*-(1,2,3-trimethoxy-10-morpholino-9-oxo-5,6,7,9-tetrahydrobenzo[a]heptalen-7-yl)formamide (3.20c): Yellow needles; ^{1}H NMR (500 MHz, $CDCl_3$): δ 8.18 (s, 1H), 7.29 (d, *J* = 2.6 Hz, 1H), 7.26 (s, 1H), 7.21 (d, *J* = 7.7 Hz, 1H), 6.77 (d, *J* = 11.0 Hz, 1H), 6.54 (s, 1H), 4.72 (dt, *J* = 12.0, 7.0 Hz, 1H), 3.95 (s, 3H), 3.91 (s, 3H), 3.66 (s, 3H), 3.56 (ddd, *J* = 12.3, 6.1, 3.2 Hz, 2H), 3.32 (ddd, *J* = 12.3, 6.1, 3.2 Hz, 2H), 2.53 (dd, *J* = 13.3, 6.4 Hz, 1H), 2.45 (td, *J* = 13.1, 6.8 Hz, 1H), 2.27 (tt, *J* = 13.0, 6.7 Hz, 1H), 1.99 – 1.84 (m, 4H); ^{13}C NMR (125 MHz, $CDCl_3$): δ 181.2, 160.6, 158.0, 153.3, 151.3, 148.8, 141.6, 136.1, 134.4, 134.2, 129.6, 125.7, 118.1, 107.3, 66.7, 61.5, 61.4, 56.1, 50.4, 49.0, 37.1, 30.0; ESIMS *m/z* 441.30 $[M+H]^+$ (calcd for $C_{24}H_{29}N_2O_6^+$, 441.20).

(*S*)-*N*-(1,2,3-trimethoxy-10-(4-methylpiperazin-1-yl)-9-oxo-5,6,7,9-tetrahydrobenzo[a]-heptalen-7-yl)formamide (3.20d): Yellow solid; ^{1}H NMR (500 MHz, $CDCl_3$) δ 8.20 (s, 1H), 7.27 (d, *J* = 11.0 Hz, 1H), 6.80 (d, *J* = 11.0 Hz, 1H), 6.54 (s, 1H), 4.73 (1H), 3.95 (s, 3H), 3.91 (s, 3H), 3.66 (s, 3H), 3.59 (s, 2H), 3.45 (s, 2H), 2.69 (s, 4H), 2.56 – 2.49 (m, 1H), 2.42 (s, 4H), 2.28 (1H), 1.91 (1H). ^{13}C NMR (125 MHz, $CDCl_3$) δ 181.2, 160.6, 158.0, 153.2, 151.3, 148.7, 141.6, 139.7, 136.2, 134.2, 129.5, 125.8, 118.4, 107.3, 61.5, 61.4, 56.1, 54.8, 50.4, 48.3, 45.9, 37.2, 30.0. HRMS *m/z* 454.2343 $[M+H]^+$ (calcd for $C_{25}H_{32}N_3O_5^+$, 454.2336).

(*S*)-*N*-(1,2,3-trimethoxy-9-oxo-10-(4-phenylpiperazin-1-yl)-5,6,7,9-tetrahydrobenzo[a]-heptalen-7-yl)formamide (3.20e): Yellow solid; ^{1}H NMR (500 MHz, $CDCl_3$) δ 8.22 (s, 1H), 7.36 – 7.30 (m, 4H), 7.29 (1H), 7.00 (d, *J* = 7.8 Hz, 2H), 6.92 (t, *J* = 7.3 Hz, 1H), 6.84 (d, *J* = 11.1 Hz, 1H), 6.55 (s, 1H), 4.76 (dt, *J* = 11.3, 7.0 Hz, 1H), 3.96 (s, 3H), 3.92 (s, 3H), 3.76

(m, 2H), 3.68 (s, 3H), 3.55 (m, 2H), 3.42 (m, 4H), 2.58 – 2.42 (m, 2H), 2.29 (m, 1H), 1.92 (m, 1H).^{13}C NMR (125 MHz, $CDCl_3$) δ 181.2, 160.6, 158.0, 153.3, 151.3, 151.0, 141.7, 136.2, 134.3, 134.1, 129.5, 129.2, 125.8, 120.1, 118.1, 116.2, 116.2, 107.3, 61.5, 61.4, 56.1, 50.4, 49.2, 48.6, 37.2, 30.0. HRMS *m/z* 516.2495 $[M+H]^+$ (calcd for $C_{30}H_{34}N_3O_5^+$, 516.2493).

(*S*)-*N*-(10-(4-ethylpiperazin-1-yl)-1,2,3-trimethoxy-9-oxo-5,6,7,9-tetrahydrobenzo[a]-heptalen-7-yl)formamide (3.20f): Yellow solid; ^{1}H NMR (500 MHz, $CDCl_3$) δ 8.21 (s, 1H), 7.26 (s, 1H), 6.80 (d, *J* = 11.0 Hz, 1H), 6.54 (s, 1H), 4.75 (1H), 3.95 (s, 3H), 3.91 (s, 3H), 3.66 (s, 3H), 3.62 (s, 2H), 3.44 (s, 2H), 2.70 (s, 4H), 2.54 (m, 3H), 2.45 (1H), 2.28 (s, 1H), 1.93 (s, 1H), 1.17 (t, 3H). ^{13}C NMR (125 MHz, $CDCl_3$) δ 181.2, 160.6, 158.1, 153.2, 151.3, 148.8, 141.6, 136.3, 134.3, 129.3, 125.8, 118.3, 107.3, 61.5, 61.4, 56.1, 52.6, 52.3, 50.4, 48.4, 37.3, 30.0, 11.8; HRMS *m/z* 468.2490 $[M+H]^+$ (calcd for $C_{26}H_{34}N_3O_5^+$, 468.2493).

(*S*)-*N*-(10-(4-benzylpiperazin-1-yl)-1,2,3-trimethoxy-9-oxo-5,6,7,9-tetrahydrobenzo[a]-heptalen-7-yl)formamide (3.20g): Yellow solid; ^{1}H NMR (500 MHz, $CDCl_3$) δ 8.19 (s, 1H), 7.37 (m, 4H), 7.31 (d, *J* = 6.6 Hz, 1H), 7.26 (d, *J* = 11.0 Hz, 2H), 7.22 – 7.11 (m, 1H), 6.77 (d, *J* = 11.1 Hz, 1H), 6.54 (s, 1H), 4.74 (dt, *J* = 11.7, 6.9 Hz, 1H), 3.95 (s, 3H), 3.91 (s, 3H), 3.66 (s, 3H), 3.62 (s, 2H), 3.60 – 3.55 (m, 2H), 3.44 – 3.36 (m, 2H), 2.68 (m, 4H), 2.55 – 2.40 (m, 3H), 2.27 (tt, *J* = 13.0, 6.5 Hz, 2H), 1.89 (td, *J* = 11.7, 6.6 Hz, 1H). ^{13}C NMR (125 MHz, $CDCl_3$) δ 181.2, 160.6, 158.2, 153.21, 151.3, 148.5, 141.6, 136.2, 134.3, 129.3, 129.2, 128.4, 127.3, 125.9, 118.1, 107.3, 62.9, 61.5, 61.4, 56.1, 52.9, 50.4, 48.5, 37.3, 30.0; HRMS *m/z* 530.2653 $[M+H]^+$ (calcd for $C_{31}H_{36}N_3O_5^+$, 530.2649).

(*S*)-*N*-(10-(diethylamino)-1,2,3-trimethoxy-9-oxo-5,6,7,9-tetrahydrobenzo[a]heptalen-7-yl)formamide (3.20h): Yellow solid; ^{1}H NMR (500 MHz, $CDCl_3$): δ 8.20 (s, 1H), 7.54 (d, *J* = 7.7 Hz, 1H), 7.24 (d, *J* = 11.4 Hz, 1H), 7.14 (s, *J* = 9.2 Hz, 1H), 6.58 (d, *J* = 11.5 Hz,

1H), 6.52 (s, 1H), 4.79 – 4.68 (m, 1H), 3.95 (s, *J* = 7.2 Hz, 3H), 3.90 (s, *J* = 10.2 Hz, 3H), 3.65 (s, 3H), 3.64 – 3.55 (m, 4H), 2.54 – 2.33 (m, 3H), 2.32 – 2.15 (m, 2H), 1.96 – 1.79 (m, 2H), 1.30 (t, *J* = 6.6 Hz, 5H). ^{13}C NMR (125 MHz, $CDCl_3$): δ 179.2, 160.7, 156.0, 152.8, 151.4, 148.1, 141.6, 136.6, 134.5, 129.1, 126.4, 124.9, 111.8, 107.3, 61.4, 61.3, 56.1, 50.1, 46.2, 37.7, 30.2, 12.7; ESIMS *m/z* 427.30 $[M+H]^+$ (calcd for $C_{24}H_{31}N_2O_5^+$, 427.22).

(*S*)-*N*-(10-(benzyl(methyl)amino)-1,2,3-trimethoxy-9-oxo-5,6,7,9-tetrahydrobenzo[a]-heptalen-7-yl)formamide (3.20i): Yellow solid; ^{1}H NMR (500 MHz, $CDCl_3$): δ 8.10 (s, 1H), 8.06 (d, *J* = 8.1 Hz, 1H), 7.44 – 7.40 (m, 1H), 7.38 – 7.28 (m, 8H), 6.69 (d, *J* = 11.4 Hz, 1H), 6.53 (s, 1H), 4.94 (d, *J* = 15.7 Hz, 1H), 4.74 (dt, *J* = 11.8, 7.3 Hz, 1H), 4.68 (d, *J* = 15.7 Hz, 1H), 3.97 (d, *J* = 7.7 Hz, 1H), 3.95 – 3.93 (m, 2H), 3.91 (s, 2H), 3.65 (s, 3H), 3.06 (s, 3H), 2.50 – 2.44 (m, 1H), 2.43 – 2.36 (m, 1H), 2.19 (dt, *J* = 19.1, 6.5 Hz, 1H), 1.96 (td, *J* = 11.9, 6.4 Hz, 1H). ^{13}C NMR (125 MHz, $CDCl_3$): δ 179.9, 160.8, 157.4, 153.1, 151.3, 149.7, 141.6, 137.7, 136.8, 134.5, 131.9, 129.5, 128.9, 128.5, 127.5, 127.3, 115.1, 107.4, 61.4, 61.4, 56.7, 56.1, 50.2, 40.0, 37.4, 30.2; ESIMS *m/z* 475.30 $[M+H]^+$ (calcd for $C_{28}H_{31}N_2O_5^+$, 475.22).

(*S*)-*N*-(10-(dibenzylamino)-1,2,3-trimethoxy-9-oxo-5,6,7,9-tetrahydrobenzo[a]-heptalen-7-yl)formamide (3.20j): Yellow solid; ^{1}H NMR (500 MHz, $CDCl_3$): δ 8.03 (s, 1H), 7.37 – 7.30 (m, 10H), 7.29 – 7.25 (m, 3H), 7.12 (d, *J* = 11.2 Hz, 1H), 6.68 – 6.63 (m, 1H), 6.50 (s, 1H), 4.89 – 4.69 (m, 6H), 3.91 (s, 3H), 3.90 (s, 3H), 3.62 (s, 3H), 2.48 – 2.41 (m, 2H), 2.22 – 2.13 (m, 1H), 1.90 – 1.82 (m, 1H). ^{13}C NMR (125 MHz, $CDCl_3$): δ 180.4, 160.6, 156.4, 153.0, 151.3, 141.6, 137.0, 136.3, 134.4, 128.6, 127.9, 127.4, 127.3, 126.0, 116.0, 107.3, 61.3, 61.3, 56.1, 54.7, 50.1, 37.5, 30.1; ESIMS *m/z* 551.40 $[M+H]^+$ (calcd for $C_{34}H_{35}N_2O_5^+$, 551.25).

(*S*)-*N*-(10-amino-1,2,3-trimethoxy-9-oxo-5,6,7,9-tetrahydrobenzo[a]heptalen-7-yl)formamide (3.20k): Yellow solid; ^{1}H NMR (500 MHz, $CDCl_3$) δ 8.21 (s, 1H), 8.13 (s, 1H), 7.59 (s, 1H), 7.37 – 7.33 (m, 1H), 6.93 (d, J = 11.0 Hz, 1H), 6.55 (s, 1H), 6.18 (s, 2H), 4.84 – 4.74 (m, 1H), 3.95 (s, 3H), 3.91 (s, 3H), 3.63 (s, 3H), 2.50 (dd, J = 13.2, 6.1 Hz, 1H), 2.38 (td, J = 13.0, 6.7 Hz, 1H), 2.29 (ddd, J = 19.1, 12.5, 6.4 Hz, 1H), 1.97 (td, J = 11.8, 6.7 Hz, 1H). ^{13}C NMR (125 MHz, $CDCl_3$) δ 175.1, 160.9, 155.7, 153.1, 151.1, 150.0, 141.5, 139.2, 134.4, 132.1, 126.5, 125.4, 112.5, 107.2, 61.4, 56.1, 51.1, 37.3, 30.0; HRMS *m/z* 371.1607 $[M+H]^+$ (calcd for $C_{20}H_{23}N_2O_5^+$, 371.1601).

(*S*)-*N*-(10-(butylamino)-1,2,3-trimethoxy-9-oxo-5,6,7,9-tetrahydrobenzo[a]heptalen-7-yl)formamide (3.20l): Yellow solid; ^{1}H NMR (500 MHz, $CDCl_3$) δ 8.21 (s, 1H), 8.11 – 7.85 (m, 1H), 7.56 – 7.49 (m, 1H), 7.46 (d, *J* = 11.2 Hz, 1H), 7.31 – 7.25 (m, 1H), 6.64 (d, *J* = 11.4 Hz, 1H), 6.55 (s, 1H), 4.81 (dd, *J* = 11.6, 6.4 Hz, 1H), 3.96 (s, 3H), 3.92 (s, 3H), 3.64 (s, 3H), 3.38 (q, *J* = 7.0 Hz, 2H), 2.49 (dt, *J* = 9.9, 4.7 Hz, 1H), 2.39 (qd, *J* = 10.6, 4.5 Hz, 1H), 2.30 (dq, *J* = 12.7, 6.6 Hz, 1H), 1.98 (dq, *J* = 11.5, 6.0 Hz, 1H), 1.77 (p, *J* = 7.1 Hz, 2H), 1.50 (h, *J* = 7.4 Hz, 2H), 1.01 (t, *J* = 7.3 Hz, 3H); HRMS *m/z* 427.2232 $[M+H]^+$ (calcd for $C_{24}H_{31}N_2O_5^+$, 427.2227).

(*S*)-*N*-(10-((4-chlorophenyl)amino)-1,2,3-trimethoxy-9-oxo-5,6,7,9-tetrahydrobenzo[a]-heptalen-7-yl)formamide (3.20m): Yellow crystals; ^{1}H NMR (500 MHz, $CDCl_3$): δ 8.72 (s, 1H), 8.23 (s, 1H), 7.59 (s, 1H), 7.46 – 7.40 (m, 2H), 7.37 (d, *J* = 11.2 Hz, 1H), 7.30 (d, *J* = 8.7 Hz, 2H), 7.22 (d, *J* = 11.2 Hz, 1H), 6.56 (s, 1H), 4.88 – 4.75 (m, 1H), 3.95 (s, 3H), 3.92 (s, 3H), 3.66 (s, 3H), 2.54 (dd, *J* = 13.2, 6.1 Hz, 1H), 2.43 (td, *J* = 13.0, 6.7 Hz, 1H), 2.33 (ddd, *J* = 18.9, 12.3, 6.3 Hz, 1H), 1.98 (td, *J* = 11.7, 6.6 Hz, 1H), 1.33 – 1.25 (m, 1H). ^{13}C NMR (125 MHz, $CDCl_3$): δ 175.6, 160.7, 153.3, 151.7, 151.1, 150.6, 141.7, 138.8, 136.7,

134.2, 133.2, 131.2, 129.9, 126.4, 125.3, 125.1, 110.3, 107.3, 61.4, 61.4, 56.1, 51.1, 37.5, 30.0; ESIMS *m/z* 481.25 $[M+H]^+$ (calcd for $C_{26}H_{26}ClN_2O_5^+$, 481.15).

(*S*)-*N*-(1,2,3-trimethoxy-10-((4-methoxyphenyl)amino)-9-oxo-5,6,7,9-tetrahydrobenzo-[a]heptalen-7-yl)formamide (3.20n): Yellow solid; ^{1}H NMR (500 MHz, $CDCl_3$): δ 8.67 (s, 1H), 8.25 (s, 1H), 8.11 (d, *J* = 7.3 Hz, 1H), 7.67 (s, 1H), 7.35 (d, *J* = 11.3 Hz, 1H), 7.27 (dt, *J* = 5.2, 2.3 Hz, 3H), 7.09 (d, *J* = 11.3 Hz, 1H), 7.02 – 6.97 (m, 2H), 6.55 (s, 1H), 4.88 – 4.77 (m, 1H), 3.94 (s, 3H), 3.91 (s, 3H), 3.86 (s, 3H), 3.65 (s, 3H), 2.52 (dd, *J* = 13.0, 6.2 Hz, 1H), 2.43 (td, *J* = 12.9, 6.7 Hz, 1H), 2.34 (ddd, *J* = 19.0, 12.4, 6.4 Hz, 1H), 2.04 (td, *J* = 11.9, 6.4 Hz, 1H). ^{13}C NMR (125 MHz, $CDCl_3$): δ 175.2, 160.9, 158.0, 153.3, 153.10, 151.1, 150.5, 141.6, 139.1, 134.4, 132.1, 130.7, 126.6, 126.2, 124.6, 115.0, 110.0, 107.3, 61.4, 61.4, 56.1, 55.6, 51.2, 37.4, 30.0; ESIMS *m/z* 477.30 $[M+H]^+$ (calcd for $C_{27}H_{29}N_2O_6^+$, 477.20).

(*S*)-*N*-(1,2,3-trimethoxy-9-oxo-10-(p-tolylamino)-5,6,7,9-tetrahydrobenzo[a]heptalen-7-yl)formamide (3.20o): Yellow solid; ^{1}H NMR (500 MHz, $CDCl_3$): δ 8.74 (s, 1H), 8.25 (s, 1H), 8.01 – 7.92 (m, 1H), 7.65 (s, 1H), 7.36 (d, *J* = 11.3 Hz, 1H), 7.30 – 7.19 (m, 6H), 6.56 (s, 1H), 4.86 – 4.79 (m, 1H), 3.94 (s, 3H), 3.91 (s, 3H), 3.65 (s, 3H), 2.53 (dd, *J* = 13.0, 6.2 Hz, 1H), 2.44 (dd, *J* = 12.9, 6.8 Hz, 1H), 2.40 (s, 3H), 2.34 (ddd, *J* = 19.0, 12.4, 6.3 Hz, 1H), 2.03 (td, *J* = 12.1, 6.6 Hz, 1H). ^{13}C NMR (125 MHz, $CDCl_3$): δ 175.4, 160.9, 153.1, 152.6, 151.1, 150.5, 141.6, 139.1, 136.1, 135.4, 134.4, 132.4, 130.3, 126.6, 124.7, 124.1, 110.2, 107.3, 61.4, 61.4, 56.1, 51.2, 37.4, 30.0, 21.1; ESIMS *m/z* 461.30 $[M+H]^+$ (calcd for $C_{27}H_{29}N_2O_5^+$, 461.21).

(*S*)-*N*-(10-((4-bromophenyl)amino)-1,2,3-trimethoxy-9-oxo-5,6,7,9-tetrahydrobenzo-[a]-heptalen-7-yl)formamide (3.20p): Yellow solid; ^{1}H NMR (500 MHz, $CDCl_3$): δ 8.72 (s, 1H), 8.23 (s, 1H), 7.57 (dd, *J* = 12.0, 3.3 Hz, 3H), 7.40 – 7.34 (m, 1H), 7.27 – 7.21 (m,

3H), 7.15 (d, *J* = 5.5 Hz, 1H), 6.56 (s, 1H), 4.86 – 4.77 (m, 1H), 3.95 (s, 3H), 3.92 (s, 3H), 3.65 (s, 3H), 2.54 (dd, *J* = 13.3, 6.0 Hz, 1H), 2.42 (td, *J* = 13.0, 6.6 Hz, 1H), 2.37 – 2.29 (m, 1H), 1.97 (dd, *J* = 18.1, 11.5 Hz, 1H). ^{13}C NMR (125 MHz, $CDCl_3$): δ 175.6, 160.7, 153.3, 151.6, 151.1, 150.6, 141.7, 138.8, 137.3, 134.2, 133.3, 132.9, 126.3, 125.4, 125.4, 118.9, 110.4, 107.3, 61.5, 61.4, 56.1, 51.1, 37.5, 29.9; HRMS *m/z* 525.1018 $[M+H]^+$ (calcd for $C_{26}H_{26}BrN_2O_5^+$, 525.1020).

3.3.4.2. Synthesis of amides by new synthetic methodology

3.3.4.2.1. Synthesis of Ni-Ni PBA

$Ni(OAc)_2.4H_2O$ (1 mmol) and tri-sodium citrate (0.38 mmol) was dissolved in 20 mL of distilled water and stirred for 10 minutes to form the solution A. $K_2[Ni(CN)_4]$ (1 mmol) was dissolved in 20 mL distilled water and stirred for 10 minutes to form the solution B. The solution B was added to solution A at a time and stirred for five minutes. Sky blue precipitate of Ni-Ni PBA started appearing after five minutes. The solution was aged for 24 h at room temperature (without stirring). The precipitate was collected by centrifugation (at 12000 rpm for 10 minutes) and washed five times with water and finally with acetone. The obtained precipitate was dried at 60 °C in a hot air oven overnight (Zakaria et al., 2015).

3.3.4.2.2. Synthesis of NiO@Ni from Ni-Ni PBA

100 mg of Ni-Ni PBA was ground in a mortar pestle to get a fine powder. The powder was placed in a crucible boat and heated at 350 °C in the air for 1 h (in a tubular furnace with heating rate: 3 °C/min from 35 °C). The furnace was allowed to cool down to room temperature. The black powder was collected and denoted as NiO@Ni (Zou et al., 2016).

3.3.4.2.3. General procedure of amide synthesis

Aldehyde (1 mmol, 1 equiv.), amine (1 mmol, 1 equiv.), TBHP (4 mmol), and NiO@Ni (5 mg) were added to a round bottom flask containing 1,4-dioxane (1 ml). The reaction was refluxed at 60 ºC for 8 hours with stirring under nitrogen atmosphere. The reaction was monitored for completion by thin-layer chromatography. After completion, the reaction mixture was allowed to cool to room temperature, and the catalyst was separated by magnet. Then the reaction mixture was extracted with ethyl acetate and washed with a saturated solution of potassium carbonate. The organic layer was dried over anhydrous sodium sulfate and concentrated under vacuum. The crude product was purified with silica gel column chromatography using hexane and ethyl acetate to get the corresponding amide.

Phenyl(piperidin-1-yl)methanone (3.25a): ^{1}H NMR ($CDCl_3$, 500 MHz): δ 7.39 (s, 5H, Ar-H), 3.71 (bs, 2H), 3.336 (bs, 2H), 1.44-1.73 (m, 6H); ^{13}C NMR ($CDCl_3$, 125 MHz): δ 170.3, 136.7, 129.3, 128.4, 126.8, 48.8, 43.2, 26.6, 25.6, 24.6; ESIMS: 190 $[M+H]^+$ (Balaboina et al., 2019).

(4-Methoxyphenyl)(piperidin-1-yl)methanone (3.25b): ^{1}H NMR ($CDCl_3$, 500 MHz): δ 7.36-7.37 (m, 2H, Ar-H), 6.89-6.91 (m, 2H, Ar-H), 3.82 (s, 3H), 3.47-3.68 (m, 4H), 1.58-1.68 (m, 6H); ^{13}C NMR ($CDCl_3$, 125 MHz): δ 170.3, 160.5, 128.9, 128.7, 113.6, 55.3, 24.7; ESIMS: 220 $[M+H]^+$ (Lu et al., 2016).

(3-Bromophenyl)(piperidin-1-yl)methanone (3.25c): ^{1}H NMR ($CDCl_3$, 500 MHz): δ 7.27-7.33 (m, 2H, Ar-H), 7.53-7.54 (m, 2H, Ar-H), 3.70 (br s, 2H), 3.33 (br s, 2H), 1.53-1.71 (m, 6H); ^{13}C NMR ($CDCl_3$, 125 MHz): δ 168.5, 138.5, 132.4, 130.1, 129.9, 125.3, 122.6, 48.7, 43.2, 26.5, 25.6, 24.5; ESIMS: 268.10 $[M+H]^+$ (Messa et al., 2018).

(4-Chlorophenyl)(piperidin-1-yl)methanone (3.25d): ^{1}H NMR ($CDCl_3$, 500 MHz): δ 7.34-7.40 (m, 4H, Ar-H), 3.71 (br s, 2H), 3.34 (br s, 2H), 1.53-1.70 (m, 6H); ^{13}C NMR ($CDCl_3$,

125 MHz): δ 169.2, 135.4, 134.9, 128.7, 128.4, 48.8, 43.2, 26.6, 25.6, 24.5; ESIMS: 224 $[M+H]^+$ (Lu et al., 2016).

(2-Hydroxyphenyl)(piperidin-1-yl)methanone (3.25e): ^{1}H NMR ($CDCl_3$, 500 MHz): δ 9.70 (br s, 1H), 7.29-7.32 (t, 1H, Ar-H), 7.22-7.24 (d, 1H, Ar-H), 6.98-7.00 (d, 1H, Ar-H), 6.819-6.851 (t, 1H, Ar-H), 3.64-3.66 (t, 4H), 1.63-1.71(m, 6H); ^{13}C NMR ($CDCl_3$, 125 MHz): δ 170.9, 159.2, 132.5, 128.3, 118.6, 118.1, 117.5, 47.0, 26.3, 24.7; ESIMS: 206.15 $[M+H]^+$ (O'Mahony and Pitts, 2010).

(2-Nitrophenyl)(piperidin-1-yl)methanone (3.25f): ^{1}H NMR ($CDCl_3$, 500 MHz): δ 8.18-8.20 (m, 1H, Ar-H), 7.69-7.72 (m, 1H, Ar-H), 7.54-7.58 (m, 1H, Ar-H), 7.38-7.40 (m, 1H, Ar-H), 3.77 (d, 2H), 3.16-3.18 (t, 2H), 1.47-1.78 (m, 6H); ^{13}C NMR ($CDCl_3$, 125 MHz): δ 166.3, 145.2, 134.4, 133.5, 129.6, 128.0, 124.7, 47.9, 42.7, 25.8, 25.1, 25.0; ESIMS: 235.15 $[M+H]^+$ (Krabbe et al., 2016).

(4-Nitrophenyl)(piperidin-1-yl)methanone (3.25g): ^{1}H NMR ($CDCl_3$, 500 MHz): δ 8.28-8.30 (d, 2H, Ar-H), 7.56-7.58 (m, 2H, Ar-H), 3.74 (br s, 2H), 3.30 (br s, 2H), 1.54-1.72 (m, 6H); ^{13}C NMR ($CDCl_3$, 125 MHz): δ 167.9, 148.2, 142.7, 127.8, 123.9, 48.7, 43.2, 26.5, 25.5, 24.4; ESIMS 235.15 $[M+H]^+$ (Sureshbabu et al., 2019).

(4-Chlorophenyl)(morpholino)methanone (3.25h): ^{1}H NMR ($CDCl_3$, 500 MHz): δ 7.34-7.42 (m, 4H, Ar-H), 3.44-3.75 (m, 8H); ^{13}C NMR ($CDCl_3$, 125 MHz): δ 169.3, 136.0, 133.6, 128.9, 128.7, 66.8, 48.3, 42.8; ESIMS: 226.15 $[M+H]^+$ (Lu et al., 2016).

(4-Chlorophenyl)(pyrrolidin-1-yl)methanone (3.25i): ^{1}H NMR ($CDCl_3$, 500 MHz): δ 7.40-7.43 (m, 2H, Ar-H), 7.28-7.33 (m, 2H, Ar-H), 3.54-3.59 (m, 2H), 3.33-3.37 (m, 2H), 1.80-1.90 (m, 4H); ^{13}C NMR ($CDCl_3$, 125 MHz): δ 168.5, 135.7, 135.5, 128.6, 128.4, 49.6, 46.3, 26.4, 24.4; ESIMS: 210.10 $[M+H]^+$ (Inagawa et al., 2019).

(3-Bromophenyl)(pyrrolidin-1-yl)methanone (3.25j): ^{1}H NMR ($CDCl_3$, 500 MHz): δ 7.28-7.67 (m, 4H, Ar-H), 3.63-3.66 (t, 2H), 3.41-3.44 (t, 2H), 1.88-2.01 (m, 4H); ^{13}C NMR ($CDCl_3$, 125 MHz): δ 168.0, 139.2, 132.8, 130.2, 129.9, 125.7, 122.4, 49.6, 46.3, 26.4, 24.4; ESIMS: 254.10 $[M+H]^+$ (Inagawa et al., 2019).

***N*-Benzyl-4-chloro-*N*-methylbenzamide (3.25k):** ^{1}H NMR ($CDCl_3$, 500 MHz): δ 7.28-7.43 (m, 8H, Ar-H), 7.18 (s, 1H, Ar-H), 4.52-4.76 (d, 2H), 2.88-3.05 (d, 3H); ^{13}C NMR ($CDCl_3$, 125 MHz): δ 170.5, 135.7, 134.5, 128.7, 128.6, 128.4, 128.3, 127.7, 126.6, 55.2, 50.9, 37.0, 33.4; ESIMS: 260.15 $[M+H]^+$ (Ren et al., 2016).

(3-Bromophenyl)(morpholino)methanone (3.25l): ^{1}H NMR ($CDCl_3$, 500 MHz): δ 7.56-7.58 (m, 2H, Ar-H), 7.28-7.35 (m, 2H, Ar-H), 3.44-3.78 (m, 8H); ^{13}C NMR ($CDCl_3$, 125 MHz): δ 168.7, 137.3, 133.0, 130.2, 130.2, 125.6, 122.7, 66.8, 48.2, 42.7; ESIMS: 270 $[M+H]^+$ (Cederbalk et al., 2017).

3-Bromo-*N*,*N*-diethylbenzamide (3.25m): ^{1}H NMR ($CDCl_3$, 500 MHz): δ 7.53-7.55 (m, 2H, Ar-H), 7.26-7.32 (m, 2H, Ar-H), 3.54 (br s, 2H), 3.26 (br s, 2H), 1.13-1.27 (m, 6H); ^{13}C NMR ($CDCl_3$, 125 MHz): δ 169.5, 139.2, 132.2, 130.0, 129.4, 124.8, 122.5, 43.3, 39.4, 14.2, 12.9; ESIMS: 256 $[M+H]^+$ (Kumpulainen and Pohjakallio, 2014).

***N*-Benzyl-4-chlorobenzamide (3.25n):** ^{1}H NMR ($CDCl_3$, 500 MHz): δ 7.33-7.76 (m, 9H, Ar-H), 6.38 (s, 1H, N-H), 4.66-4.67 (d, 2H); ^{13}C NMR ($CDCl_3$, 125 MHz): δ 166.3, 137.9, 137.8, 132.7, 128.9, 128.4, 128.0, 127.8, 44.3 ; ESIMS: 246.20 $[M+H]^+$ (Chen and Wu, 2019).

***N*-Benzylbenzamide (3.25o):** ^{1}H NMR ($CDCl_3$, 500 MHz): δ 7.81-7.82 (m, 2H, Ar-H), 7.32-7.52 (m, 8H, Ar-H), 6.57 (br s, 1H, N-H), 4.65-4.66 (d, 2H); ^{13}C NMR ($CDCl_3$, 125 MHz):

δ 167.4, 138.2, 134.4, 131.6, 128.8, 128.6, 127.9, 127.6, 127.0, 44.1; ESIMS: 212.20 $[M+H]^+$ (Nordstrøm et al., 2008).

***N*-Benzyl-3-bromobenzamide (3.25p):** ^{1}H NMR ($CDCl_3$, 500 MHz): δ 7.95 (t, 1H, Ar-H), 7.71-7.73 (m, 1H, Ar-H), 7.63-7.65 (m, 1H, Ar-H), 7.30-7.40 (m, 6H, Ar-H), 6.46 (br s, 1H, N-H), 4.64-4.65 (d, 2H); ^{13}C NMR ($CDCl_3$, 125 MHz): δ 165.9, 137.8, 136.4, 134.5, 130.2, 130.2, 128.9, 128.0, 127.8, 125.6, 122.8, 44.3 ; ESIMS: 290.10 $[M+H]^+$ (Ai et al., 2018).

***N*-Benzyl-4-nitrobenzamide (3.25q):** ^{1}H NMR ($CDCl_3$, 500 MHz): δ 8.32-8.34 (d, 2H, Ar-H), 8.12-8.13 (d, 2H, Ar-H), 7.24-7.38 (m, 5H, Ar-H), 4.51-4.52 (d, 2H); ^{13}C NMR ($CDCl_3$, 125 MHz): δ 165.1, 149.5, 140.4, 139.6, 129.3, 128.8, 127.8, 127.4, 124.1, 44.3; ESIMS: 255.15 $[M-H]^+$ (Jamalifard et al., 2019).

***N*-Butyl-4-chlorobenzamide (3.25r):** ^{1}H NMR ($CDCl_3$, 500 MHz): δ 7.72-7.70 (d, 2H, Ar-H), 7.41-7.39 (d, 2H, Ar-H), 6.20 (NH), 3.47-3.30 (2H), 1.64-1.53 (2H), 1.46-1.34 (2H), 0.98-0.93 (3H); ^{13}C NMR ($CDCl_3$, 125 MHz): δ 166.5, 137.5, 133.2, 128.8, 128.3, 39.4, 31.2, 20.0, 13.6; ESIMS: 212.15 $[M+H]^+$ (Yu et al., 2019).

Methyl benzoyl-*L*-valinate (3.25s): ^{1}H NMR ($CDCl_3$, 500 MHz): δ 7.82-7.84 (d, 2H, Ar-H), 7.45-7.55 (m, 3H, Ar-H), 6.66-6.67 (d, 1H, NH), 4.80-4.82 (dd, 1H), 3.79 (s, 3H), 2.25-2.33 (m, 1H), 1.00-1.04 (m, 6H); ^{13}C NMR ($CDCl_3$, 125 MHz): δ 172.7, 167.3, 134.2, 131.8, 128.6, 127.1, 57.4, 52.3, 31.7, 19.0, 18.0; ESIMS: 236.20 $[M+H]^+$ (Reddy et al., 2008).

Methyl (4-chlorobenzoyl)-*L*-valinate (3.25t): ^{1}H NMR ($CDCl_3$, 500 MHz): δ 7.76-7.77 (m, 2H, Ar-H), 7.43-7.45 (m, 2H, Ar-H), 6.63-6.64 (d, 1H, NH), 4.77-4.79 (dd, 1H), 3.80 (s, 3H), 2.27-2.31 (m, 1H), 0.99-1.03 (m, 6H); ^{13}C NMR ($CDCl_3$, 125 MHz): δ 172.6, 166.3, 138.0, 132.5, 128.9, 128.5, 57.5, 52.3, 31.6, 19.0, 18.0; ESIMS: 270.20 $[M+H]^+$ (Malavašič et al., 2011).

Methyl benzoyl-*L*-leucinate (3.25u): ^{1}H NMR ($CDCl_3$, 500 MHz): δ 7.78-7.79 (m, 2H, Ar-H), 7.39-7.49 (m, 3H, Ar-H), 6.65 (s, 1H, NH), 4.84-4.88 (m, 1H), 3.75 (s, 3H), 1.66-1.76 (m, 3H), 0.95-0.98 (m, 6H); ^{13}C NMR ($CDCl_3$, 125 MHz): δ 173.8, 167.1, 133.9, 131.7, 128.6, 127.1, 52.4, 51.1, 41.8, 25.0, 22.8, 22.1; ESIMS: 250.20 $[M+H]^+$ (Reddy et al., 2008).

3.3.4.3. Synthesis of C-10 amide derivatives of gloriosine

To a solution of **3.20k** (0.2 mmol, 74 mg) in dioxane (1 ml), was added 0.25 mmol of respective aldehyde, followed by TBHP (0.8 mmol), and NiO@Ni (5 mg). The reaction was refluxed at 60 ºC for 8 hours with stirring under nitrogen atmosphere. Then reaction mixture was partitioned between ethyl acetate and saturated solution of sodium bicarbonate three times. The organic layers were combined and passed through anhydrous sodium sulphate, followed by concentration under reduced pressure. The crude product was purified with silica gel column chromatography using hexane and ethyl acetate to get the corresponding amide.

(*S*)-*N*-(7-formamido-1,2,3-trimethoxy-9-oxo-5,6,7,9-tetrahydrobenzo[a]heptalen-10-yl)benzamide (3.26a): ^{1}H NMR (500 MHz, $CDCl_3$) δ 10.32 (s, 1H), 9.24 (d, J = 10.8 Hz, 1H), 8.22 (s, 1H), 7.99 (d, J = 6.9 Hz, 2H), 7.68 (s, 1H), 7.61 (t, J = 7.4 Hz, 1H), 7.54 (dd, J = 9.2, 6.9 Hz, 3H), 6.55 (s, 1H), 4.78 (dt, J = 12.7, 6.8 Hz, 1H), 3.95 (s, 3H), 3.91 (s, 3H), 3.67 (s, 3H), 2.55 (dd, J = 13.6, 6.4 Hz, 1H), 2.44 – 2.37 (m, 1H), 2.29 (tt, J = 12.9, 6.5 Hz, 1H), 1.92 (td, J = 11.9, 6.6 Hz, 1H). ^{13}C NMR (125 MHz, $CDCl_3$) δ 178.1, 166.4, 160.8, 153.8, 152.1, 151.3, 145.7, 141.7, 139.7, 138.6, 134.3, 134.0, 132.6, 130.1, 129.0, 127.5, 125.5, 121.1, 107.3, 61.5, 61.4, 56.1, 51.1, 36.8, 29.8.

(*S*)-2-fluoro-*N*-(7-formamido-1,2,3-trimethoxy-9-oxo-5,6,7,9-tetrahydrobenzo[a]-heptalen-10-yl)benzamide (3.26b): ^{1}H NMR (500 MHz, $CDCl_3$) δ 10.76 (d, J = 13.3 Hz, 1H), 9.28 (d, J = 10.8 Hz, 1H), 8.26 (s, 1H), 8.17 (td, J = 7.8, 1.9 Hz, 1H), 7.78 – 7.72 (m,

1H), 7.62 – 7.56 (m, 1H), 7.53 (d, *J* = 10.8 Hz, 1H), 7.36 (td, *J* = 7.4, 1.1 Hz, 1H), 7.25 (dd, *J* = 11.3, 8.9 Hz, 1H), 6.57 (s, 1H), 4.86 (dt, *J* = 12.8, 6.5 Hz, 1H), 3.98 (s, 3H), 3.94 (s, 3H), 3.70 (s, 3H), 2.58 (dd, *J* = 13.9, 6.3 Hz, 1H), 2.45 (dt, *J* = 13.9, 6.6 Hz, 1H), 2.41 – 2.26 (m, 1H), 1.96 (d, *J* = 9.5 Hz, 1H). ^{13}C NMR (125 MHz, $CDCl_3$) δ 178.1, 162.9, 161.5, 160.6, 159.5, 153.8, 152.1, 151.4, 145.8, 141.7, 139.9, 138.2, 134.5, 134.4, 134.0, 132.1, 130.7, 125.6, 125.1, 125.1, 121.8, 121.5, 121.4, 116.7, 116.5, 107.3, 61.6, 61.4, 56.1, 50.9, 36.9, 29.9. ^{19}F NMR (471 MHz, $CDCl_3$) δ -111.68 (tq, *J* = 13.0, 6.1 Hz).

(*S*)-*N*-(7-formamido-1,2,3-trimethoxy-9-oxo-5,6,7,9-tetrahydrobenzo[a]heptalen-10-yl)acetamide (3.26c): ^{1}H NMR (500 MHz, $CDCl_3$) δ 9.39 (s, 1H), 9.04 (d, *J* = 10.9 Hz, 1H), 8.22 (s, 1H), 7.54 (s, 1H), 7.47 (d, *J* = 10.9 Hz, 1H), 6.61 (d, *J* = 7.3 Hz, 1H), 6.56 (s, 1H), 4.77 (dt, *J* = 12.4, 6.8 Hz, 1H), 3.96 (s, 3H), 3.93 (s, 3H), 3.66 (s, 3H), 2.57 (dd, *J* = 13.6, 6.3 Hz, 1H), 2.43 (td, *J* = 13.2, 6.8 Hz, 1H), 2.33 (s, 3H), 2.33 – 2.27 (m, 1H), 1.87 (td, *J* = 12.1, 6.5 Hz, 1H). ^{13}C NMR (125 MHz, $CDCl_3$) δ 177.8, 170.1, 160.4, 153.8, 151.4, 151.3, 145.5, 141.8, 139.1, 138.5, 133.8, 130.2, 125.5, 120.7, 107.2, 61.5, 61.4, 56.1, 51.0, 37.1, 29.7, 25.7.

(*S*)-*N*-(7-formamido-1,2,3-trimethoxy-9-oxo-5,6,7,9-tetrahydrobenzo[a]heptalen-10-yl)octanamide (3.26d): ^{1}H NMR (500 MHz, $CDCl_3$) δ 9.39 (s, 1H), 9.07 (d, *J* = 10.8 Hz, 1H), 8.22 (s, 1H), 7.56 (d, *J* = 2.9 Hz, 1H), 7.47 (d, *J* = 11.0 Hz, 1H), 6.55 (s, 1H), 4.77 (dt, *J* = 12.8, 6.9 Hz, 1H), 3.96 (s, 3H), 3.92 (s, 3H), 3.66 (s, 3H), 2.55 (dt, *J* = 19.7, 7.1 Hz, 4H), 2.42 (td, *J* = 12.9, 7.3 Hz, 1H), 2.30 (tt, *J* = 13.0, 6.5 Hz, 1H), 1.88 (td, *J* = 11.8, 6.6 Hz, 1H), 1.77 (p, *J* = 7.5 Hz, 4H), 1.45 – 1.24 (m, 10H), 0.90 (t, *J* = 6.7 Hz, 3H). ^{13}C NMR (125 MHz, $CDCl_3$) δ 177.8, 173.3, 160.4, 153.8, 151.4, 151.3, 145.6, 141.8, 139.0, 138.5, 133.8, 130.1, 125.6, 120.7, 107.2, 61.5, 61.4, 56.1, 51.0, 38.7, 37.0, 31.7, 29.8, 29.1, 29.0, 25.4, 22.6, 14.1.

3.3.5. *In-vitro* cytotoxicity studies

3.3.5.1. General procedure for cytotoxicity (MTT) assay

The cytotoxicity study was performed using the MTT assay. The cells lines were purchased from National Cancer Institute (NCI), Bethesda USA, and cultured according to the provided protocol. The cells were grown in a CO_2 incubator (Esco) at 37 °C in a humidified atmosphere (98% humidity) of 95% air and 5% CO_2. In this assay, the cells were plated in a 96-well plate for 12 hours. Then, the cells were treated with different concentrations (5, 10, 50, 100, and 500 nM) of test compounds for a duration of 48 h. After incubation, 10 µL of MTT dye (2.5 mg/mL in PBS) was added to each well and incubated for 4 h at 37 °C. Then, the supernatant was aspirated and purple MTT-formazan crystals obtained were dissolved in 150 µL DMSO. The absorbance of this colored solution was measured at a wavelength of 570 Nm. Each experiment was repeated three times and data was expressed as mean ± SD of three independent experiments (Goel et al., 2021).

3.3.5.2. Nuclear staining and fluorescence microscopy

The A549 cells were treated with 50, 100 and 500 nM concentrations of gloriosine and 500 nM of colchicine for 24 h. After treatment, cells were collected, washed twice with PBS and fixed in 400 µL of cold acetic acid: methanol (1:3, v/v) overnight at 4 °C. The next day, cells were washed and dispensed in 50 µL of fixing solution. After that, the cells were spread out on a clean slide and allowed to dry at room temperature overnight. The cells were stained with DAPI (5 µg/mL in 0.01 M citric acid and 0.45 M disodium phosphate containing 0.05% Tween 20) for 30 min at room temperature, then the slides were rinsed with distilled water followed by washing with PBS. While the slide was still wet, 40 µL of mounting fluid (PBS: glycerol, 1:1) was poured over it, then sealed with a glass coverslip. Cells were observed under a microscope for any nuclear morphological changes that occur during apoptosis. For

phase-contrast microscopy, cells were simply photographed using a microscope after treatment (Goel et al., 2021).

3.3.5.3. Scratch assay for migration studies

The cell migrations studies were performed in A549 cells. A549 cells were treated with mitomycin C to inactivate cell proliferation. The cells were scratched with a 200-µl sterile microtip, and washed three times with phosphate-buffered saline (PBS), supplemented with fresh medium and treated with 50, 100 and 500 nM concentrations of gloriosine and 500 nM of colchicine for 24 h. Images of the cells were taken after 24 h of incubation (Sharma et al., 2015).

3.3.6. Molecular docking studies

Molecular docking studies were performed using AutoDock 4.2 to study the molecular interactions between gloriosine and tubulin protein (PDB: 4O2B) (Morris et al., 2009). The pdb2pqr webserver was used to assign the right protonation state to the residues. All the water molecules, ligands, and ions were removed. Non-polar hydrogen atoms were removed, and Gasteiger charges were added using M.G.L Tools 1.5.7.rc1. AutoDock employs Autogrid4 to compute maps. The docking study was performed using Lamarckian Genetic Algorithm (LGA). The docking was performed with 100 runs, 150 population sizes, 27,000 number of generations, and 2,500,000 number of energy evaluations. It employs a “semiempirical free energy force field” to evaluate conformations at the time of docking simulation. The docking protocol validation was done by re-docking the co-crystallized ligand and calculating RMSD between docked pose and co-crystallized ligand. The docked pose was visualized by Discovery studio 2019 for studying interactions. Upon successful completion of docking

simulation, the best confirmation was selected with the best binding energy in the largest cluster of 2.0 Å.

3.3.7. Molecular dynamics simulation of gloriosine-tubulin complex

Molecular dynamics (MD) simulation of gloriosine-tubulin complex was carried out using the Desmond package (D.E. Shaw Research, New York, USA) with inbuilt optimized potentials for liquid simulations (OPLS 2005) force field (Bowers et al., 2006). The gloriosine-tubulin complex was obtained from the Autodock. Before performing the MD simulation, the solvated system was prepared. The complex was solvated using an open TIP3P water model in periodic boundary condition of a cubic box with dimensions 12 X 12 X 12 Å. The overall negative charge of the system was neutralized using adding sodium ions. The desired electrically neutral system for simulation was built with 0.15 M NaCl. The relaxation of the system was performed by implementing the steepest descent and the limited memory Broyden-Fletcher-Goldfarb-Shanno algorithm with a threshold of 2.0 kcal mol^{-1} (John et al., 2015). The simulation was performed under an NPT ensemble for 100 ns implementing the Berendsen thermostat and barostat methods. A constant temperature of 310 K was maintained across the simulation run using the Noose-Hoover thermostat algorithm and the pressure of 1 atm was maintained using the Martyna-Tobias-Klein Barostat algorithm (Bowers et al., 2006; Evans and Holian, 1985). The cut-off value of 9.0 Å was set to analyse the short-range coulombic interactions using the short-range method. The long-range coulombic interactions were handled using the smooth particle mesh ewald method. The tolerance value for long range interactions was set to 10^{-9} which was implemented by the SHAKE algorithm. The final production run was carried out for 100 ns and the trajectory sampling was done at 100 ps. The trajectories obtained from the following MD run were

analysed for protein and ligand RMSD, protein root-mean square fluctuation (RMSF), and H-bond interactions.